INVADE

*Smart system of renewable energy storage based on **IN**tegrated E**V**s and b**A**tteries to empower mobile, **D**istributed and centralised **E**nergy storage in the distribution grid*

Deliverable nº:	**D6.2**
Deliverable name:	**Battery techno-economics tool**
Version:	**1.0**
Release date:	**15/03/2018**
Dissemination level:	**Public** (Public, Confidential)
Status:	**Approved** (Draft, Peer-reviewed, Submitted, Approved)
Author:	**Ari Hentunen, Juha Forsström, Samppa Jenu, Saara Tuurala, Aino Manninen - VTT** **Sigurd Bjarghov - NTNU**

Document history:

Version	Date of issue	Content and changes	Edited by
0.1	28/02/2018	First draft version	Ari Hentunen
0.2	04/03/2018	Executive summary added	Ari Hentunen
1.0	15/03/2018	Peer-reviewed version	Ari Hentunen

Peer reviewed by:

Partner	Reviewer
UPC	Pol Olivella-Rosell
eSmart	Stig Ødegaard Ottesen

Deliverable beneficiaries:

WP / Task
WP5 / Tasks 5.3 & 5.4
WP8 / Tasks 8.3 & 8.5
WP10 / all tasks
WP6 / Task 6.1

Table of contents

Abbreviations and Acronyms

Acronym	Description
AC	Alternating Current
BMS	Battery Management System
BRP	Balance Responsible Party
C&I	Commercial and Industrial
CC	Constant Current
CC-CV	Constant-Current–Constant-Voltage
CHP	Combined Heat and Power
CV	Constant Voltage
DOD	Depth Of Discharge
DSO	Distribution System Operator
ECM	Equivalent Circuit Model
EEC	Electrical Equivalent Circuit
EMS	Energy Management System
EOL	End Of Life
EV	Electric Vehicle
FO	Flexibility Operator
kWmax	Maximum Load
LFP	Lithium Iron Phosphate
LIB	Lithium Ion Battery
LMO	Lithium Manganese Oxide
LNO	Lithium Nickel Oxide
LTO	Lithium Titanate Oxide
MPC	Model Predictive Control
NCA	Nickel Cobalt Aluminium
NMC	Nickel Manganese Cobalt
OCV	Open Circuit Voltage
PCS	Power Conversion System
PV	Photovoltaic
RUL	Remaining Useful Life
SCADA	System Control and Data Acquisition
SEI	Solid Electrolyte Interphase
SOC	State of Charge

Acronym	Description
SOE	State of Energy
SOH	State of Health
SOS2	Special Ordered Sets of type 2
USABC	US Advanced Battery Consortium

Symbols

Symbol	Description
a	Slope of efficiency curve
c	Degradation unit cost of a battery
c_0	Specific investemnt cost of a battery
C_b	Procurement cost of a battery [€]
C_{deg}	Degradation cost of a battery [€]
E^{ch}	Charged energy [kWh]
E^{dch}	Discharged energy [kWh]
E_n	Energy capacity of a battery [kWh]
I	Current [A]
I_{spec}	Specified current at which the nominal efficiency is obtained [A]
K	Investment cost of a battery [€]
P_b	Terminal power of a battery [W]
P^{ch}	Maximum charging power limit [W]
P^{dch}	Maximum discharging power limit [W]
R	Internal resistance of a battery [Ω]
S_2	Special ordered sets of type 2
T_s	Time step [h]
U	Voltage [V]
U_{oc}	Open-circuit voltage [V]
V_t	Binary variable
δ	Depth of discharge [%]
$\Delta\delta$	Cycle depth [%]
Φ	Cycle life
η	Efficiency [%]
η_b	Efficiency of a battery [%]
η^{ch}	Efficiency during charging [%]
η^{dch}	Efficiency during discharging [%]
η^{rt}	Roundtrip efficiency [%]
η^{rt}_{spec}	Roundtrip efficiency at a specified rate [%]
ρ	Inverse of a cycle life

Symbol	Description
σ	Power [W]
θ	State of charge [%]
Θ	State of charge [Ah]
ψ	State of energy [%]
Ψ	State of energy [kWh]

Glossary

C-rate	A measure of the rate at which a battery is discharged relative to the manufacturer's rated capacity in ampere-hours. It is also related to the discharge time. For example, if the battery's rated capacity is 40 Ah, then 1C rate is 40 A and the battery is empty after a 1-hour discharge, 2C rate is 80 A and the battery is empty after a 0.5-hour discharge, and C/4 rate is 10 A and the battery is empty after a 4-hour discharge.
Calendar life	The length of time a battery can undergo some defined operation before failing to meet its specified end-of-life criteria.
Capacity	The capacity of a battery expresses the maximum available ampere-hours when a full battery is discharged at a certain C-rate until the cut-off voltage is reached.
Cycle	A sequence of a discharge followed by a charge, or a charge followed by a discharge under specified conditions.
Cycle life	The number of cycles, each to specified discharge and charge termination criteria under a specified charge and discharge regime, that a battery can undergo before failing to meet its specified end-of-life criteria.
Cycle depth	Cycle depth (ΔDOD or ΔSOC) describes the depth of a discharge-charge cycle. Cycle depth is usually expressed in percentage.
Degradation stress factor	Degradation stress factors are all the operation practices or circumstances that accelerate the degradation in battery and thus shorten the lifetime of the cell. Also known as the state of health stress factors.
Depth of discharge	The depth of discharge is a measure of how much charge has been discharged from a full battery. It is usually expressed in percents, but is sometimes expressed also in amperehours.
Discharge rate	See *C-rate*.
E-rate	Similar to *C-rate*, but in terms of power against energy capacity. That is, E-rate describes the rate of discharge power relative to the manufacturer's rated energy capacity in kilowatt-hours. For example, a battery that is discharged at a rate of 1E is fully discharged in an hour.
End of life	The stage at which a battery is not anymore capable to meet its performance criteria regarding capacity or power.
Internal impedance	Opposition to the flow of an alternating current at a particular frequency at a specified state of charge and temperature.
Internal resistance	Opposition to direct current flow in a battery. It is the sum of the ionic and electronic resistances of a battery.

Nominal operating voltage	The average voltage of a battery, as specified by the manufacturer, during discharging at a specified rate and temperature.
Open-circuit voltage	The equilibrium voltage of a battery at a specified state of charge and temperature when there is no current flowing.
Polarization	The voltage deviation from the equilibrium voltage under loading, i.e., when current is flowing.
Self discharge	The process by which the available capacity of a battery decreases spontaneously due to undesirable chemical side reactions or short circuits within a cell.
State of charge	The state of charge is a measure of how much charge is left in a battery. It is a ratio of the present charge and the full charge, and it is usually expressed in percents.
State of energy	The state of energy is a measure of how much energy is left in a battery. It is a ratio of the available stored energy and the nominal energy capacity. It can be expressed in kilowatt-hours and in percents.
State of health	The state of health is a measure of aging. It can be defined for capacity fade and power fade. Typically a battery is considered to be at its end of life when the state of health has decreased to 80%.
Tapering	Tapering refers to the reduction of current and power when the battery approaches fully-charged or fully-discharged state. The high and low cut-off voltages at cell level shall not be exceeded, and hence, the current needs to be reduced when the first cell reaches the cut-off voltage.
Thermal runaway	Thermal runaway occurs in Li-ion batteries when the rate of internal heat generation caused by the exothermic reactions exceeds the rate at which the heat can be expelled. Eventually, the temperature rises rapidly and the battery catches fire and burns at a very high temperature. The fire may catch nearby cells, and eventually, the whole battery may burn down.

Executive summary

Batteries are capable of providing high flexibilty due to their inherent fast dynamics combined with fast power-electronic-converter based control. Even though batteries can be used in relatively wide temperature range and deep-discharged without permanent damage, the rate of degradation varies depending on the usage and operating conditions. This rate of degradation has a high effect on the operating cost of the storage, and consequently, to the total cost of ownership of the storage and profitability of the business case.

This deliverable presents a simplified battery techno-economic model that will be included in the flexibility management allocation and operation algorithm developed in Task 5.4 *Design and program the flexibility management operation algorithm*. The basic battery modelling principles were already included in D5.3 *Simplified battery operation and control algorithm*, whereas this deliverable adds several functionalities such as additional power constraints and the cost of degradation, which are essential for the flexibility management operation algorithm to work properly. If the cost of degradation is not taken into account in the optimization algorithm, the battery will often be used in such cases that are not economically profitable. Moreover, this deliverable addresses the technical and economical aspects of energy storage systems such as the performance and lifetime characteristics as well as the past and future cost estimates. Furthermore, the parameter extraction process is described in detail and methods to evaluate key model parameters such as efficiency based on the data sheets are provided.

The updated, final version of the battery techno-economics tool will be exposed in D6.5 *Advanced battery techno-economics tool* (M24).

1 Introduction

This deliverable presents a simplified battery techno-economic model that will be included in the flexibility management allocation and operation algorithm, which is developed in Task 5.4 *Design and program the flexibility management operation algorithm.* A simplified version of this flexibility management allocation and operation algorithm is described in detail in D5.3 *Simplified battery operation and control algorithm* [1]. The basic battery modelling principles were already included in D5.3, whereas this deliverable adds several functionalities such as additional power constraints and the cost of degradation. If the cost of degradation is not taken into account in the optimization algorithm, the battery will often be used in such cases that are not economically profitable once the battery degradation is valued into the costs. Therefore, it has a high impact on the usage and lifetime of a battery, and hence, the overall profitability of a business case. Moreover, this deliverable addresses in detail the performance and lifetime characteristics of different lithium-ion (Li-ion) battery chemistries and the parameter extraction process. The implementation of these algorithms is performed in Task 8.3 *Implementation of the Flexibility Cloud flexibility management algorithms, functions, and monitoring & control dashboards,* and the simplified algorithms will be described in detail in D8.2 *Cloud based flexibility management system: Flexibility Cloud, phase 2 (M18): Simplified Flexibility management operation*.

The background for this document is presented in deliverables D5.3 *Simplified battery operation and control algorithm* [1], D5.2 *Methods for assessing the flexibility in distribution grids* [2], D6.1 *Storage system dimensioning and design tool* [3], D4.1 *Overall INVADE architecture* [4], D4.2 *INVADE architecture of pilots* [5], and D10.1 *Pilot specifications* [6].

The objective of this deliverable is to provide a tool that optimizes the battery operation in such a way that the maximum economic value can be obtained. In order to achieve this, the degradation mechanisms and phenomenons that are affecting the performance need to be identified and characterized. Batteries have very complex ageing characteristics with many stress factors and interdependencies that affect the rate of ageing. These stressors need to be characterized in order to be able to provide limits and constraints for battery operation to ensure long lifetime. This identification and characterization of degradation stress factors is performed in Task 6.2 and reported in D6.3 *Simplified state of health diagnostics tool* [7]. The main findings are utilized in this report. Together with the proposed modelling methods for the cost of degradation, the

optimal operation in terms of performance, lifetime, and economic value can be obtained. Moreover, battery system modelling methods and parameter extraction methodology are proposed that can be used in the flexibility management operation algorithm.

The updated, final version of the battery techno-economics tool will be exposed in D6.5 *Advanced battery techno-economics tool* (M24). In D6.5, the parameter extraction methodology will be adapted to the pilots and the tool integration to Task 5.4 and D5.4 *Advanced optimal battery operation and control algorithm* (M24) will be described. In addition, more advanced modelling methods will be included, e.g., more stress factors could be included into the model, which would likely improve the control of battery life cycle economics. Furthermore, currently all battery models are defined as open-loop systems, i.e., they take no feedback from the process. Instead, they rely on knowledge available beforehand over the entire planning horizon. Model predictive control (MPC) is capable of taking feedback from the real world and still utilize optimization as a method of making operational plans. The use of MPC looks promising, and it is being considered to be included in D6.5.

2   Lithium-ion batteries

Lithium-ion batteries (LIBs) are electrochemical energy storages with complex nonlinear characteristics and interdependencies. The fundamental operation of LIBs is based on a reversible process, in which lithium ions transfer from a positive electrode to a negative electrode during charging, and vice versa during discharging. There are several electrode compositions for anode and cathode with different characteristics regarding performance, lifetime, and cost. These materials and compositions are discussed in more detail in D6.1 *Storage system dimensioning and design tool* [3].

In this chapter, generic performance characteristics of LIBs are presented to provide information for the control and optimization of use, which is addressed in Chapter 4. This chapter is organized as follows. Characteristics and performance are presented in Section 2.1. degradation processes and safety characteristics are presented in Section 2.2, and the degradation stress factors are presented in Section 2.3. The end of life (EOL) criteria are discussed in Section 2.4, and the use of batteries in second-life applications are discussed in Section 2.5. These topics are discussed only briefly in this report, and they are addressed in more detail in D6.3 *Simplified state of health diagnostics tool* [7].

2.1   Characteristics and performance

Active anode and cathode material composition and characteristics dictate the capacity and open-circuit voltage (OCV) of a battery, and thus, they also determine the baseline for the energy density and inherent safety features. Other inherent characteristics of a battery cell are the internal impedance, entropy change, and heat capacity. Besides these, the internal structure, geometry, and casing affect the thermal performance, and thus, the current rating of a cell. All these characteristics together dictate the energy capacity, efficiency and power capability of a battery.

Depending on the desired performance characteristics, the battery cell can be optimised for either energy or power. Energy-optimised cells have high energy density and moderate or low power capability, while power-optimised cells have high power capability and moderate or low energy density. In battery-electric vehicles, plug-in electric vehicles, and stationary energy storage applications typically energy-optimised cells are used, while in hybrid electric vehicles and in some stationary power-buffering applications power-optimised cells are typically used. Power-optimised cells have very small internal

impedance, which results in low heat generation and high power capability as well as high efficiency when loaded with medium power.

Each battery chemistry has a unique OCV curve and a voltage window. The specified maximum and minimum voltages should not be exceeded in any case as it may cause increased rate of degradation and even cell decomposition and permanent damage. Therefore, high and low cut-off voltage are specified for each cell to ensure safe operation and long lifetime. The controller algorithm must be capable to prevent the voltage to reach these cut-off voltages during use. This can be implemented by setting limitations for the usable state of charge (SOC) window as well as discharge power when approaching fully discharged state and charge power when approaching fully charged state.

Ideally, all stored chemical energy would be converted to electrical energy. However, polarization losses occur when a load current passes through the electrodes. These polarization losses consist of ohmic polarization, activation polarization, and concentration polarization. Ohmic polarization is caused by the resistivity of the actual materials such as metal plates and contacts, activation polarization drives the electrochemical reaction at the electrodes, and concentration polarization is caused by the concentration differences of the reactants and products at the electrode surface and in the bulk as a result of mass transfer [8]. Polarization effects consume part of the total energy as heat losses and thus reduce the efficiency of the conversion.

Internal impedance has a strong effect on the performance of a cell. Because of internal impedance, a voltage drop is present during discharging. This voltage drop is typically called ohmic polarization or *IR* drop, and it follows the Ohm's law, i.e., it is proportional to the magnitude of the load current. The total internal impedance of a cell is the sum of the ionic resistance of the electrolyte, the electronic resistances of the active mass, the current collectors and electrical tabs of the electrodes, and the contact resistance between the active mass and the current collector [8].

Example charge–discharge voltage profiles of commercial lithium manganese oxide (LMO), lithium nickel manganese cobalt (NMC), lithium iron phosphate (LFP), and lithium nickel cobalt aluminum (NCA) cells using constant-current–constant voltage (CC–CV) charging and constant-current (CC) discharging at a rate of 1C[1] are shown in Figure 1,

---

[1] Definition of C-rate as well as other battery-specific definitions can be found in the Glossary (beginning of the document).

where the x-axis shows the capacity in mAh and the y-axis the associated voltage. The upper curves are charging profiles and the lower curves are discharging profiles. It should be noted that the cells have different nominal capacities. In order to make a proper comparison, the capacities should be normalised. The area between the charge and discharge curves represents the energy losses during a full cycle. These losses reduce the efficiency of the conversion and are converted to heat that needs to be dissipated.
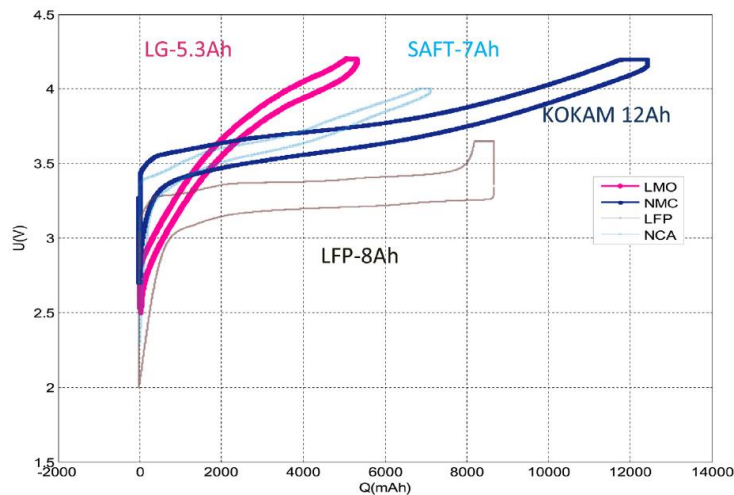

Figure 1: Voltage profile examples for different LIB chemistries. [9]

The presence of polarization losses can be seen as a difference between the OCV and the terminal voltage during loading. As the polarization effects increase with increasing current, the low cut-off voltage is reached earlier when discharging with higher rates. This is known as the rate effect. However, the capacity is not lost, but is usable once the voltage has recovered. Full relaxation takes hours to complete.

Batteries are very sensitive to temperature. Too low temperature results in poor performance and low efficiency, while too high temperature results in increased rate of degradation and even decomposition and safety risks. All these characteristics cause constraints and limitations for the usage in order to achieve safe operation and long lifetime.

A summary of the performance characteristics of the most common LIB technologies are given in [10] and shown in Table 1. Performance of different LIB chemistries were compared in [11] and [12], and the results are summarised in Table 2 and Table 3, respectively. In general, the technology choice depends on the application-specific requirements and constraints, and hence, on the weighing of different characteristics.

Table 1. Characteristics of different LIB chemistries. [10]

	Lithium Iron Phosphate	Lithium Manganese Oxide	Lithium Titanate	Lithium Cobalt Oxide	Lithium Nickel Cobalt Aluminum	Lithium Nickel Manganese Cobalt
Cathode chemistry descriptor	LFP	LMO	LTO	LCO	NCA	NMC
Specific energy (Wh/kg)	80–130	105–120	70	120–150	80–220	140–180
Energy density (Wh/L)	220–250	250–265	130	250–450	210–600	325
Specific power (W/kg)	1400–2400	1000	750	600	1500–1900	500–3000
Power density (W/L)	4500	2000	1400	1200–3000	4000–5000	6500
Volts (per cell) (V)	3.2–3.3	3.8	2.2–2.3	3.6–3.8	3.6	3.6–3.7
Cycle life	1000–2000	>500	>4000	>700	>1000	1000–4000
Self-discharge (% per month)	<1%	5%	2–10%	1–5%	2–10%	1%
Cost (per kWh)	$400–$1200	$400–$900	$600–$2000	$250–$450	$600–$1000	$500–$900
Operating temperature range (°C)	−20 to +60	−20 to +60	−40 to +55	−20 to +60	−20 to +60	−20 to +55

Table 2. Comparison of performance of different LIB chemistries from [11].

Chemistry (Shorthand)	Safety	Energy	Power	Life	Cost	Summary
	Scale 1-5 with 5 Best					
Lithium Manganese Oxide (LMO)	3	4	3	3	4	Versatile technology with good overall performance & cost
Lithium Iron Phosphate (LFP)	3	3	4	4	3	Similar to LMO, but slightly more power & less energy
Lithium Nickel Cobalt Aluminum (NCA)	1	3	4	4	2	Good for power applications; poor safety & high cost per kWh
Lithium Titanate (LTO)	5	2	5	5	2	Excellent power & cycle life; high cost per kWh
Lithium Nickel Manganese Cobalt (NMC)	3	4	4	4	4	Versatile technology with good overall performance & cost

Table 3. Comparison of performance of different LIB chemistries from [12].

Characteristics	Li-ion battery chemistries				
	NCA	NMC	LMO	LFP	LTO
Specific Energy	++[a]	++	+	-	-
Specific Power	++	+	+	+	+
Safety	-	+	+	++	++
Performance	+	+	-	+	++
Lifetime	++	+	-	++	++
Cost	-	+	+	+	-

a. "++" very good performance, "+" good performance, "-" average performance

2.1.1 Capacity

Battery cell specification provides a nominal or rated capacity expressed in ampere-hours at specified conditions, typically at around 25 °C and 1C or lower rate. It expresses the maximum available ampere-hours when a full battery is discharged at the specified

C-rate until the cut-off voltage is reached. The real usable capacity depends on the temperature, rate, and state of health (SOH).

In grid-storage applications, the capacity is typically defined in terms of energy, i.e., kilowatt-hours (kWh). In some cases, the installed capacity might differ from the usable capacity. In these cases, the SOC range or voltage range have been constrained for one or the other end or for both ends. The reason for this might be, e.g., to increase the expected lifetime, to avoid certain operation areas, to provide reserve capacity to cope with capacity fade due to ageing, or to comply with the hardware specification of the power conversion system (PCS) or other equipment.

The rate effect and the temperature effect on the discharge characteristics are illustrated in Figure 2. It can be seen that in these test conditions the rate effect is notable but not very significant for low and medium C-rates. In Figure 2, the difference in capacity between C/2 and 2C rates is approximately 5%. Moreover, the temperature effect is small too for temperature range of 25–40 $°$C. For higher temperatures, the usable capacity increases, but it comes at the expense of a higher rate of degradation, and hence, reduced lifetime.
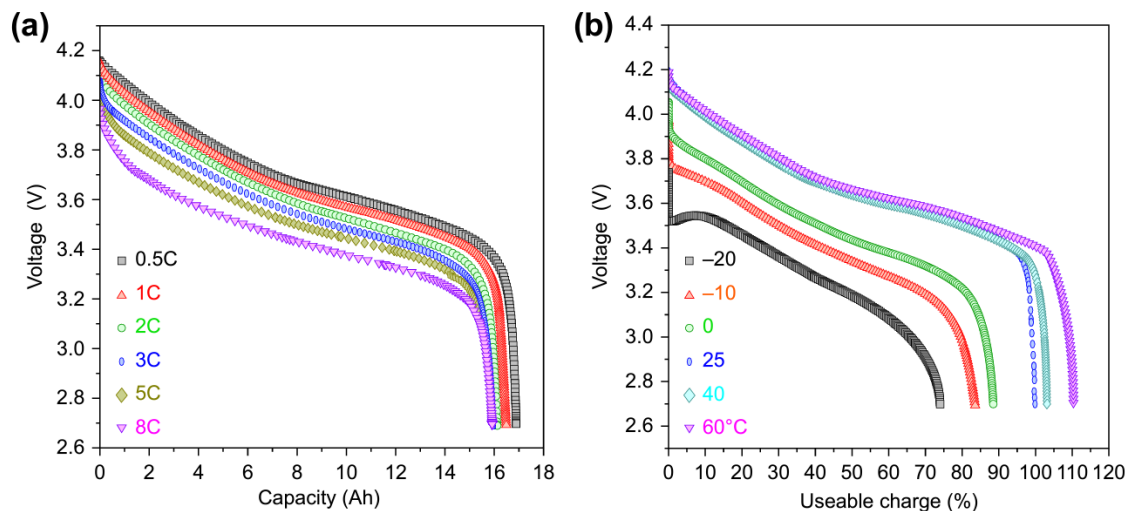

Figure 2: Discharge characteristics of a commercial Kokam 17 Ah NMC cell. (a) Characteristics at different rates and room temperature. (b) Characteristics at different temperatures at a rate of C/2. [13]

The effect of the C-rate on the maximum surface temperature of high-energy and high-power cells were studied in [14]. The results for cylindrical 18650 cells are shown in Figure 3. A linear relation between the C-rate and the maximum surface temperature can be observed. Similar behaviour was found for pouch cells [14]. The cell form factors are described in more detail in D6.1 [3].
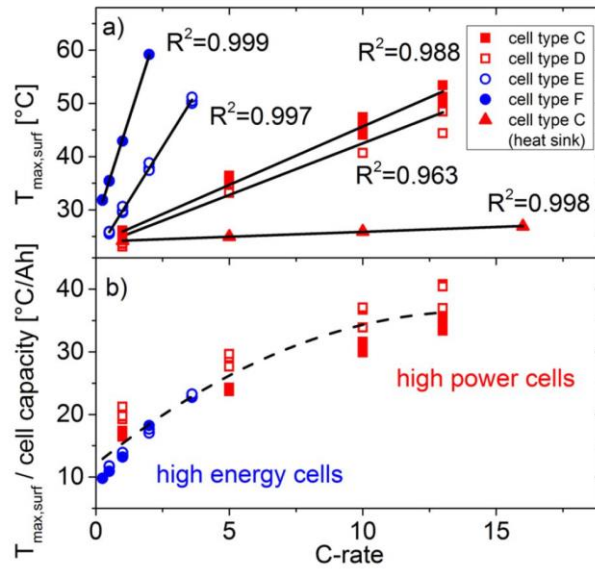
Figure 3. a) Maximum temperatures on the surface of high-power (type C and D) and high-energy (type E and F) 18650 cells without heat sink. b) Data from (a) normalized to cell capacity. All high-energy and high-power cells are indicated in blue and red, respectively. [14]

2.1.2 Impedance

The internal impedance of a battery changes as a function of temperature, rate, and ageing. Nominal values are typically given at room temperature. At colder temperatures, the impedance increases and the efficiency decreases, and at higher temperatures, the impedance decreases and the efficiency increases. The effects of temperature and SOC on the dynamic resistance of a commercial 40-Ah NMC cell are illustrated in Figure 4.
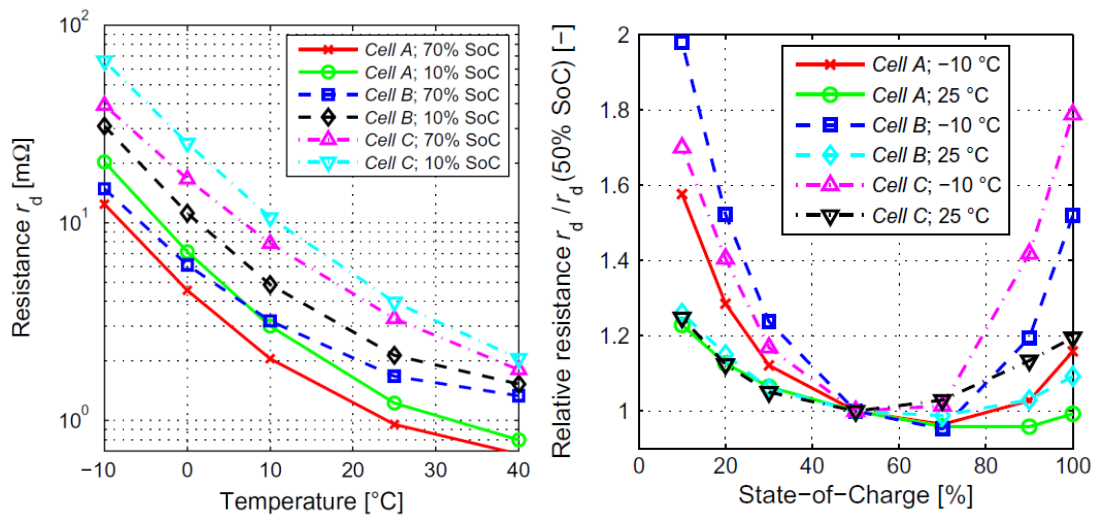

Figure 4: Dynamic resistance r_d characteristics of a Kokam 40-Ah NMC cell [15]. In the right panel, the resistances are normalized to 50% SOC to better illustrate the effect of SOC at different temperatures and SOH. That is, all impedances have unity magnitude at 50% SOC.

2.1.3   Rate capability and power capability

The rate capability of a battery cell is mainly determined by the internal impedance and thermal properties of the battery. Internal resistance opposes current flow and causes voltage drop and irreversible heat generation. The continuous and peak current ratings are typically determined based on heating. When discharging a full battery with a rated continuous discharge rate at rated temperature, the battery temperature should stay within the specified range. However, after discharging at a rated current, the battery needs time to cool down, or at least the consecutive charging must be done at a low rate, in which case the heat generation must be lower than the heat dissipation in order for the battery to cool down. The rate at which a battery cell can be discharged and charged repetitively without rest times for several hours is typically much lower than the rated continuous current. The use of the specified peak current or power typically results in a high rate of heating, and therefore, the use of peak power is strictly limited for short periods.

Manufacturers of grid-storage batteries as well as grid integrators often use a different way than cell manufacturers to define the rated continuous current or power for their energy storages. These ratings may be lower than the ratings of the cell manufacturer in order to resemble better the more continuous use of grid storages and to ensure long lifetime and stable thermal behaviour through the whole lifetime.

2.1.4   Efficiency

The instantaneous efficiency of a battery is dictated by the current, the internal resistance, and the OCV, as follows:

$$\eta = 1 - \frac{R}{U_{oc}} I \tag{1}$$

where U_{oc} is the OCV, R is the internal resistance, and I is the discharge current. However, because the OCV cannot be measured directly during loading, roundtrip energy efficiency is typically used in determining efficiency. The roundtrip energy efficiency η^{rt} is defined as the ratio of the discharged energy E^{dch} to the charged energy E^{ch}:

$$\eta^{rt} = \frac{E^{dch}}{E^{ch}} \tag{2}$$

Because of the complex and nonlinear impedance and OCV characteristics of LIBs, the actual energy efficiency depends on the rate and duration of the loading, the SOC, the temperature, and the ageing of the battery.

The roundtrip energy efficiency can be approximated with the following equation:

$$\eta^{\text{rt}} = \frac{1 - \dfrac{R}{U_{\text{oc}}} I}{1 + \dfrac{R}{U_{\text{oc}}} I} \tag{3}$$

where R and U_{oc} are average values of the internal resistance and OCV, respectively, during discharge and charge. Therefore, the efficiency can be represented as a function of rate, as follows:

$$\eta^{\text{rt}} = \frac{1 - a \cdot I}{1 + a \cdot I} \tag{4}$$

where a is the slope of the one-way efficiency during discharge and charge. A base value for a can be calculated based on the battery's data sheet, where the roundtrip efficiency at a specified rate is typically provided, as follows:

$$a = \frac{1 - \eta^{\text{rt}}_{\text{spec}}}{1 + \eta^{\text{rt}}_{\text{spec}}} \cdot \frac{1}{I_{\text{spec}}} \tag{5}$$

where $\eta^{\text{rt}}_{\text{spec}}$ is the specified roundtrip efficiency and I_{spec} is the corresponding current. The average one-way efficiency as a function of current during charging or discharging is then the square-root of the roundtrip efficiency:

$$\eta^{\text{ch}}_{\text{b}} = \eta^{\text{dch}}_{\text{b}} = \sqrt{\frac{1 - a \cdot I}{1 + a \cdot I}} \tag{6}$$

This methodology can be used to roughly estimate the roundtrip efficiency of a battery at different rates purely based on the data provided by the battery specification. The method is very much simplified, and hence, it does not take into account the effect of temperature and other factors that influence the internal resistance of a battery. The method provides fairly accurate results for low rates, which do not heat up the battery significantly. However, for high rates, this model provides too low efficiency grades, mainly because the internal heating and temperature-dependency of the internal resistance is not taken into account.

The rate has a high impact on the efficiency. Typically the roundtrip energy efficiency of a full discharge–charge cycle of a large Li-ion battery at room temperature is higher than 97% for low rates less than or equal to C/3. The extrapolated roundtrip energy efficiency curves based on the above equations for specified efficiency values from 99% to 95% and a specified rate of C/3 are shown in Figure 5.
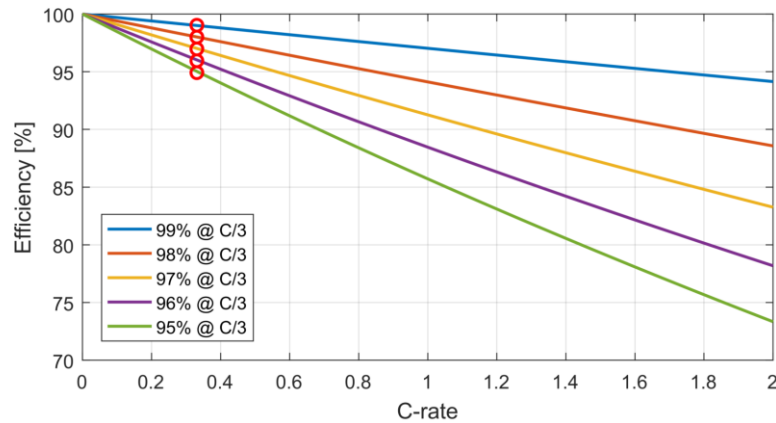

Figure 5: Extrapolated roundtrip energy efficiency curves specified at a rate of C/3. Red circles mark the specified efficiency at the specified rate.

Impedance curves are typically almost flat in the mid-SOC area from 20-80%. Therefore, in that area, the SOC affects the efficiency mostly via the OCV slope, which is dependent on the battery chemistry. As the OCV decreases with decreasing SOC, the efficiency decreases with decreasing SOC as well. Outside the mid-SOC range, especially below 20% SOC, the impedance characteristics rise significantly, which reduces the efficiency directly. Furthermore, the efficiency may decrease as a result of ageing. This is a consequence of the tendency of the impedance to increase due to ageing.

Roundtrip energy efficiencies of different LIB technologies were reported by Peters et al. in [16]. They have gathered efficiency grades of batteries from manufacturers' data sheets and research articles. The obtained efficiency grades for different LIB technologies are shown in Figure 6. The segment labelled *Li-ion* represents the results from papers that did not disclose the exact cell chemistry. The results show large variation even within same chemistries. However, the rate and temperature at which the efficiency is reported is different among the data sources, which is likely the main reason for this large variation. Nevertheless, the reported median values (91–95%) represent fairly typical values for LIBs under real-life use and conditions. However, these median efficiencies should not be used as typical or representative values of each technology in technology comparisons.
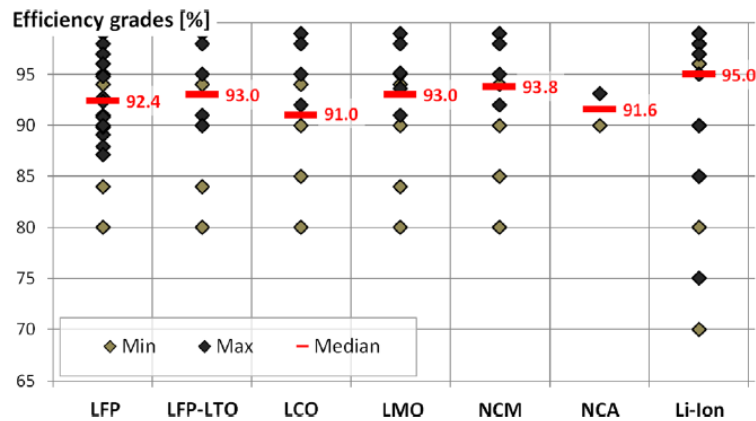
Figure 6: Comparison of battery efficiencies from different studies. [16]

2.2   Degradation processes and performance degradation

The degradation process in LIB is a complex combination of electrochemical and mechanical processes, which lead to capacity decrease and power fading. Most of these processes cannot be studied independently as they occur simultaneously at similar timescales and interact with each other. Ageing processes can be divided into two groups: ageing during use and aging during storage. In other words: ageing related to cycle life and ageing related to calendar life.

Degradation processes take place in the battery's electrolyte, especially at the interfaces with the anode and the cathode. The ageing mechanisms strongly depend on electrodes composition. The origins of the degradation mechanisms can be either chemical or mechanical, and the mechanisms can induce for example changes in the chemical composition of the electrolyte or loss of active materials at the electrodes. The key factor in Li-ion battery ageing is the formation of the solid electrolyte interphase (SEI) layer on graphite anode. [17]

The wide range of degradation mechanism can be clustered into three degradation modes: loss of lithium inventory, loss of active anode material and loss of active cathode material [18]. A list of degradation mechanism with their causes, effects and relations to the degradation modes is presented in Figure 7.
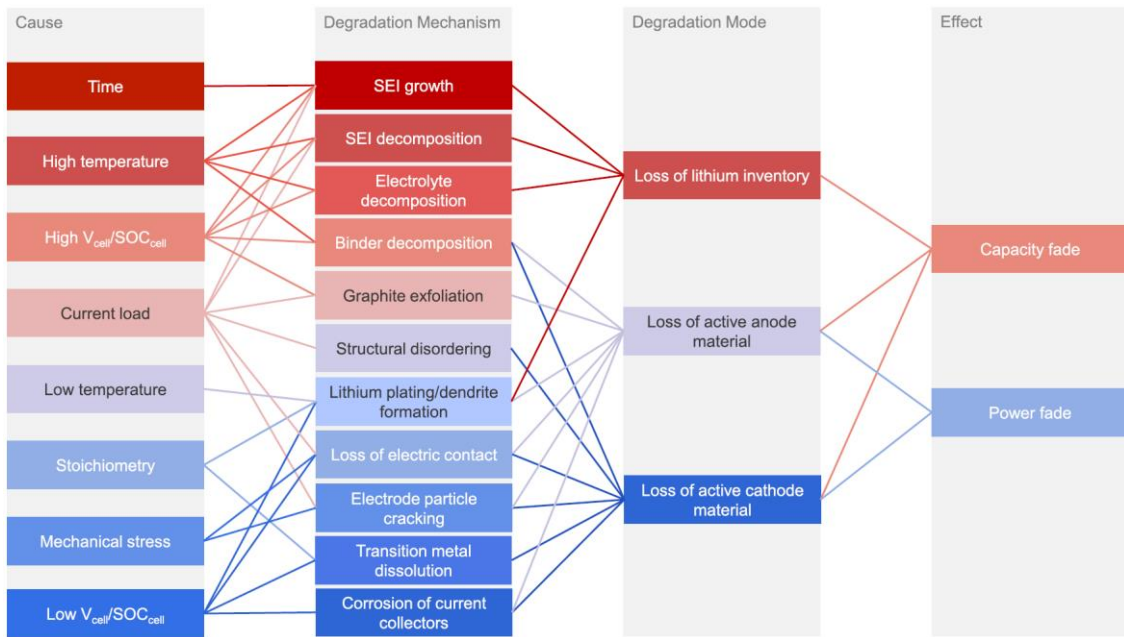
Figure 7: Causes and effects of different degradation mechanisms in Li-ion batteries. [18]

Figure 8 illustrates the temperature range of the safe temperature window for LIBs as well as the temperature grades at which the detrimental processes start to happen, possibly leading to irreversible damage of a cell and even hazardous events.
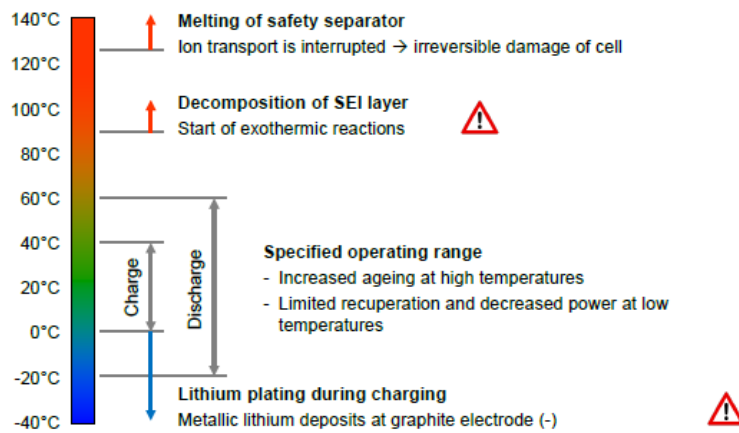

Figure 8: Safe temperature window for LIBs. [19]

2.3 Degradation stress factors

Degradation stress factors are all the operation practices or circumstances that accelerate the degradation in battery and thus shorten the lifetime of the cell. By identifying the stress factors the battery operating conditions and practices can be optimized within the application limits so that the degradation of the battery is minimized. Reference [20] identified five stressors; the environmental temperature, SOC   window,

cut-off voltages, current (C-rate), and time. The SOC window can be further divided into cycle depth (ΔDOD, i.e., equivalent to ΔSOC) and average SOC.

The degradation processes in lithium-ion batteries can be divided into two groups: degradation during cycling and degradation during storage. The degradation stress factors can be divided correspondingly: stress factors related to cycle ageing and stress factors related to calendar ageing.

Battery lifetime data has been extensively gathered from the literature in INVADE T6.2, and the main findings are exposed in D6.3 [7]. As a summary of the findings, both the battery duty cycle and the environmental conditions during operation affect the degradation rate. For different lithium ion battery chemistries the impact of different stress factors slightly varies, but the underlying degradation mechanisms are the same. The list of degradation stress factors addressed in the literature lifetime tests are shown in Table 4. These are in principle the same stressors as in [20].

Table 4. Summary of the degradation stress factors addressed in the lifetime tests of the reviewed articles in [7]. Results varied widely depending on the chemistry and even among different studies regarding the same chemistry. The values in the low-stress and optimal-range columns are very coarse generalisations based on the results.

Stressor	High stress	Low stress	Optimal range
Cycle depth (ΔDOD)	High ΔDOD	< 50%	< 30%
Temperature	High and low temperature	10–35 °C	15–30 °C
Current (C-rate)	High rate	< 1C	< C/2
SOC / voltage	High SOC / voltage	< 4 V	< 70% SOC

For most grid-storage applications, and especially for all INVADE pilots, low C-rates are employed. The P/E factor of the energy storage system (ESS) is in the order of 1 for all pilots. These low C-rates cause only low heating of the battery. Moreover, the ESSs are typically installed in temperature-controlled facilities or they include a thermal management system. Therefore, the effect of temperature can be managed, and hence, it can be regarded as having only a low impact on the lifetime of a battery. Therefore, the cycle depth can be regarded as the most important stressor for the INVADE pilots [7].

The battery manufacturers typically have a chart that includes the expected cycle lifetime as a function of ΔDOD. However, these charts are typically confidential, and therefore, they cannot be easily obtained from public sources. Some results based on experimental

research in universities and research institutes are available (e.g. [21]), though, but they typically do not have very many data points. Recently, Peters et al. [16] published charts for several LIB chemistries. The charts were based on a mathematical function combined with battery manufacturers' data. However, these charts were calculated from low number of data points and by assuming a specific shape of the curve, and hence, there is not much experimental evidence on the quality and reliability of these curves.

To obtain comprehensive understanding on the effect of cycle depth on battery cycle life, data from different literature sources were gathered in D6.3 *Simplified battery state of health diagnostics tool* [7], and the results are combined in Figure 9. To be able to compare the results, the data sets were normalised based on the cycle life with 100% ΔDOD. In practice, the cycle life (Φ) at a given ΔDOD ($\Delta\delta$) is first multiplied by ΔDOD to obtain the cycle life in equivalent full cycles (FCE). The FCE is then divided by the cycle life at 100% ΔDOD (Φ_{fc}) to obtain the normalised cycle life:

$$\Phi_{normalised} = \frac{\Phi \times \Delta\delta}{\Phi_{fc}} \qquad (7)$$

Unity in y-axis represents the case in which no lifetime extension can be found, i.e., ΔDOD cannot be regarded as a stress factor. It can be seen that the results vary significantly. However, a common finding is that the cycle lifetime is extended if the ΔDOD is less than 50%. Moreover, most results from the literature indicate also fair extension between 50–80% DOD.
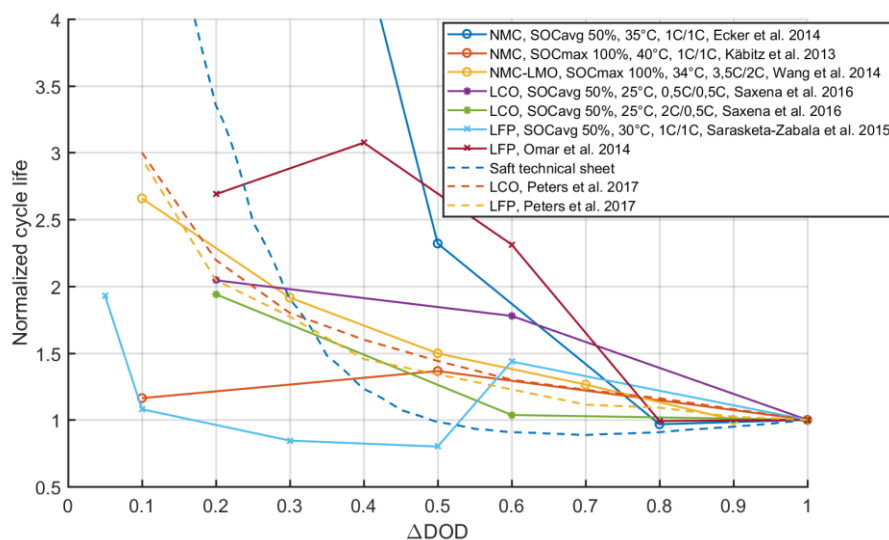

Figure 9. Normalized cycle life of different types of Li-ion cells as a function of ΔDOD. The data were gathered from the following sources: [22], [23], [24], [25], [26], [21], [27], [16].

A generic model for the effect of ΔDOD on the cycle life was derived in D6.3 [7]. The NMC-LMO data set from Wang et al. [28] was selected to be a basis for the model, because it is close to average among all the included data sets and a representative set as NMC-LMO and NMC batteries will be used in the pilots (Section 3.7). It is also close to the curves utilized by Peters et al. [29]. An exponential function was fit to the data. The data fitting is shown in Figure 10, and the resulting exponential fit is presented in Equation (8):

$$\Phi_{normalized} = 2.371 \times e^{-2.438 \times \Delta\delta} + 0.7929 \tag{8}$$

where $\Phi_{normalized}$ is the normalised cycle life of the battery and $\Delta\delta$ is the cycle depth.
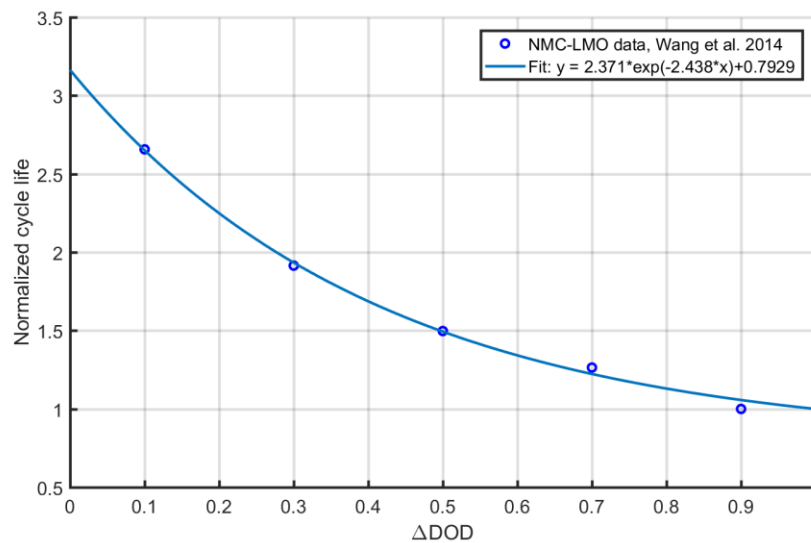

Figure 10. An exponential model fit to ΔDOD - cycle life data from Wang et al. [28].

2.4 End of life

When the battery can no longer meet its performance requirements, it has reached its EOL, and it has to be removed from the application. Being able to properly define this point is important, because it affects both the system performance and safety. If the battery has degraded too much, it may not be able to respond to the requirements set by the application where the battery is used. Also the risk of a critical failure happening in the battery pack will increase when the battery degrades.

For electric vehicle (EV) batteries a typical definition for EOL is when 70–80% of the original energy capacity is remaining [30] [31]. This originates to a standard established by the US Advanced Battery Consortium (USABC) in 1996. According to this standard the EOL has been reached when either the net delivered capacity of a cell, module or

battery is less than 80% of its rated capacity or the peak power capability is less than 80% of the rated power at 80% DOD [32]. Also a more recent standard for electric road vehicle batteries, IEC 62660 [33], defines 80% as the test termination criteria for all performance indicators, including capacity and power.

For industrial applications—including stationary energy storages—the IEC 62620 [34] standard defines that the battery is at the end of its life when the remaining capacity has dropped to 60% of the rated capacity. Similar EOL criterion is defined in IEC 61960 [35] for portable applications. According to [34], the battery should last at least 500 cycles before reaching its EOL.

2.5   Second-life batteries

When EV batteries have reached their EOL criteria (80% of nominal capacity) they still retain significant amount of energy that could be used in e.g. stationary applications (EOL criteria 60% of nominal capacity). These applications include both residential and industrial applications as well as energy utility and off-grid storages. Battery history and SOH are considerable determinants in the life cycle performance of second-life battery packs. Safety of second-life batteries strongly relates to the main aging mechanism and to the history of operating parameters during the lifetime of the cell [36]. The usage profile of the second-life application is important due to their impact on the degradation and safety of the second-life battery pack. The nominal capacity drop from 80% to 60% can be within years if ∆DOD is high, whereas cycling between small ∆DOD can lead to second life time of decades [37]. However, it is still unknown if cells after a less demanding first life use are capable of showing good performance in demanding second life applications; and if batteries aged with severe first life conditions are able to provide a stable second life performance in less demanding applications. For this reason, it can be suggested that stress factors addressed in Section 2.3 should be minimised in the case of second-life batteries, thus using optimal or at least low stress operation conditions.

3 Battery storage systems

3.1 System description

Figure 11 illustrates a typical ESS including the main subsystems, whereas Figure 12 shows only the most important functional blocks, i.e., the energy storage (ES), the PCS, and the energy management system (EMS). Large batteries are typically installed in racks and placed together with PCS and other hardware in cabinets or in containers. The EMS controls the battery and the PCS based on the provided input by the user and the subsystems.
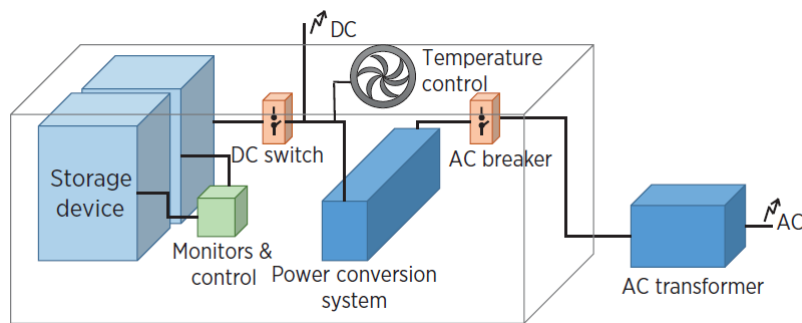

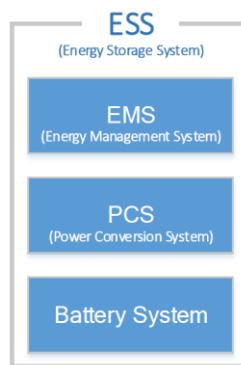*Figure 11: Energy storage system. [38]*

Figure 12. System-level layout of an ESS.

Batteries are equipped with a battery management system (BMS), which monitors the voltage of each cell as well as the system current and temperature as well as balances the cells to be in equal SOC. Other typical tasks of a BMS are the estimation of the SOC, SOH, and remaining useful life (RUL), and they typically also provide limitations for the maximum allowed current or power and give warning signals in case these limits are violated. Depending on the severity of the violation, the BMS may stop the operation to prevent permanent damage to the battery.

3.2 Energy capacity

Installed energy capacity is specified in the data sheet. Energy capacity is expressed in kWh and refers to the available energy at specified ambient temperature and power or current. Less capacity may be available at lower temperatures or at higher rates. Delivered energy at the alternating current (AC) side differs from the installed energy storage capacity.

3.3 Maximum power

Maximum charging and discharging power refers to the maximum continuous charging and discharging power at AC side. It is typically specified in the data sheet and expressed in kW. For storage applications with low P/E ratio, the maximum power is typically limited by the PCS. Some ESS data sheets provide separate specifications for the PCS and the ES. Moreover, the data sheet may specify maximum continuous current instead of power. In these cases, the system integrator should specify the maximum power at the AC side for the complete ESS.

Data sheet often provides also a peak-power rating, which may be considerably higher than the continuous rating. The battery is typically capable of providing short-time peak power of several times the nominal power, but the duration is only in the order of tens of seconds or a few minutes. For example, the data sheet of TESVOLT TS HV 70 [39] specifies a rate of 1C for continuos power and a rate of 4C for peak-power for a maximum duration of 20 s. The specified duration shall not be exceeded. In general, the loading at peak power may cause rapid heating and additional stress to the battery, and hence, it should only be used intermittently when necessary. In practice, the peak-power is often limited by the PCS, which may not be capable of such high overloads. For example, the data sheet of BYD B-Box 13.8 [40] specifies 12.8 kW continuous output power and 13.2 kW peak output power for 60 s. The overloading is so low that the peak-power rating is likely limited by the PCS.

3.4 Efficiency

The efficiency of LIBs was addressed in Section 2.1.4. When determining the energy efficiency of a storage system, one must take into account also the losses that occur in the power electronic converters and grid interface. The efficiency of the power electronic converters depends on the operating point. The efficiency is low at very low power and

high (>95%) for the most of the operating range [41]. The maximum efficiency is typically obtained in the vicinity of the nominal operating point, i.e., full power. The maximum point of the combined inverter and battery efficiency depends on the matching of the battery and the inverter, and specifically, on the nominal continuous power of the battery. The inverter is typically matched to provide the nominal power of the battery.

The efficiency characteristics of an ESS with a *P/E* ratio of 1:1 are illustrated in Figure 13, where the x-axis is normalised to the rated power, and hence, is represented in per unit (p.u.) values. The characteristics of the inverter were obtained from [41], in which a 192 kWh / 248 kW grid-storage system was modelled in detail and validated with experimental data. It is evident that in this case the efficiency is poor at low power, and consequently, that long-term operation at low power should be avoided.
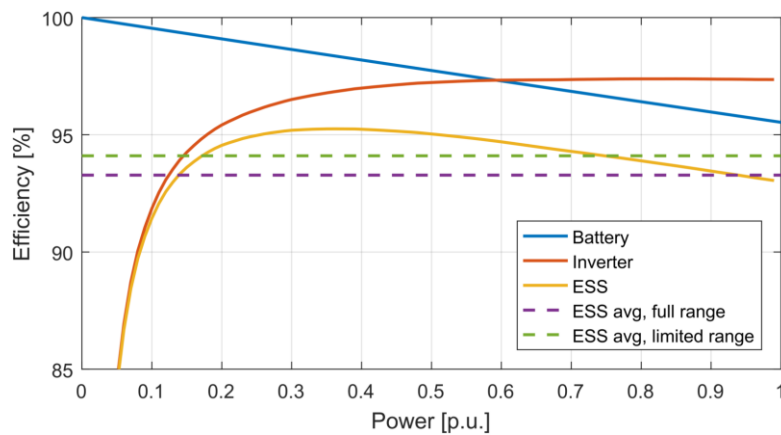

Figure 13: Typical discharge efficiency curves for an energy storage system with a P/E ratio of 1:1. The same curves apply for charging as well. The average efficiency was calculated for full range and for a limited power range from 0.06 p.u. to 1 p.u, in which the efficiency is higher than 85%.

The efficiency characteristics of a commercial SMA Sunny Tripower STP 60 inverter are and the shown in Figure 14. This state-of-the-art inverter has higher peak efficiency and average efficiency, and especially, its efficiency characteristics at low power are far superior to the former case shown in Figure 13. The corresponding efficiency curves for an ESS are shown in Figure 15.
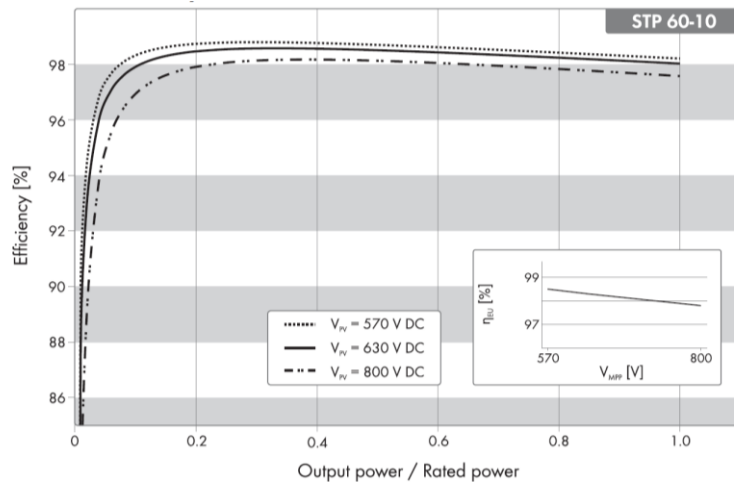
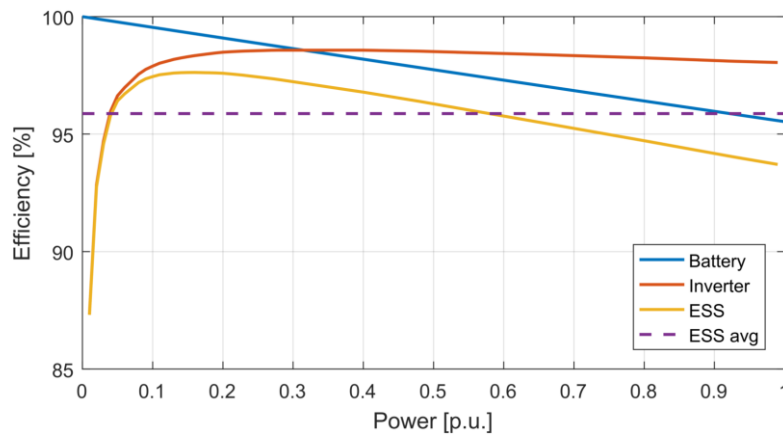*Figure 14: Efficiency chart of a SMA Sunny Tripower STP 60 inverter. [42]*

Figure 15: Efficiency curves for a SMA Sunny Tripower STP 60 inverter combined with a battery of P/E factor of 1.

3.5   Costs

Prices of battery packs for EVs and grid storage applications are declining rapidly [43]. In 2015, a decline of 8% for market leaders and 14% for others for EV battery packs was estimated in [44]. The data for these estimates and the price projections are shown in Figure 16. However, it was pointed out in [43] that the decline has been faster. Evolution of system cost made by Deutsche Bank is shown in Figure 17. Deutsche Bank estimated in 2016 in a report [45] that the average cell cost and the average stationary energy storage system cost would be 160 $/kWh and 944 $/kWh in 2018 and 150 $/kWh and 825 $/kWh in 2020, respectively. The difference between the EV battery pack cost and stationary system cost is mainly caused by the inclusion of the PCS, EMS, switches, supervisory control and data acquisition (SCADA), etc. in the stationary systems that are not present in the EVs, as well as different scales in the volumes. IRENA reported the

prices of different lithium-ion technogies for grid storage applications in 2014 and cost estimates for 2017 and 2020 in [38]. The costs are shown in Figure 18. The data and cost projections by the Deutsche Bank are considered up-to-date and useful, as it includes also the stationary storage costs. The cost of cells is converging, but the cost of ESS is still projected to be declining at an annual rate of 5–8%.
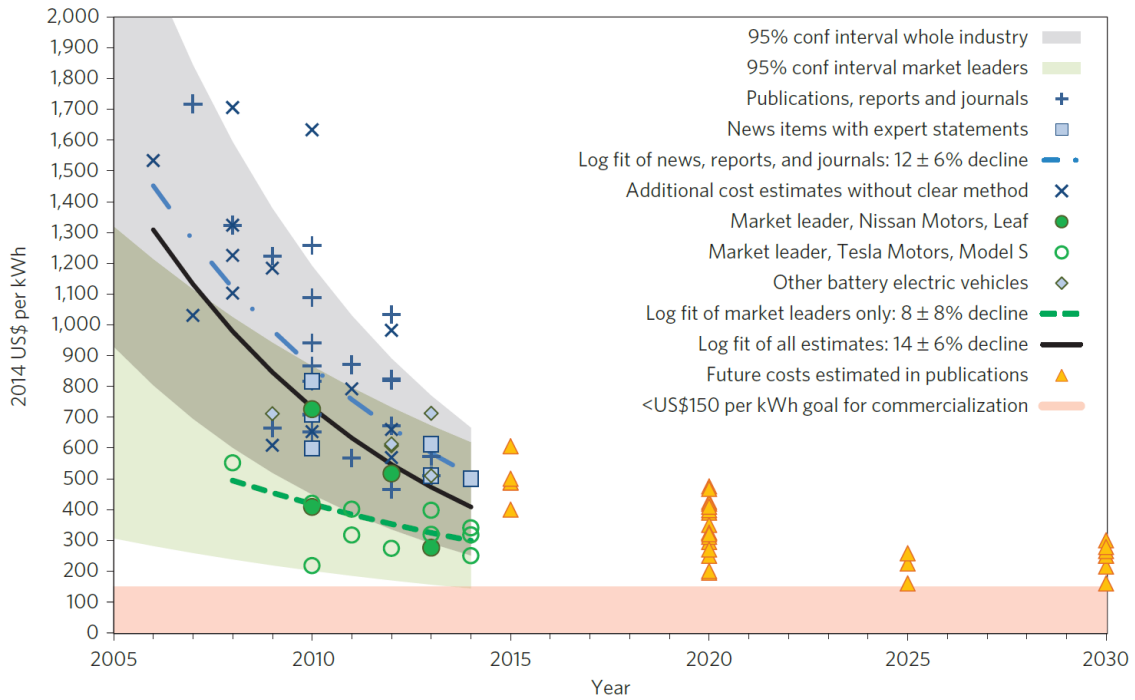

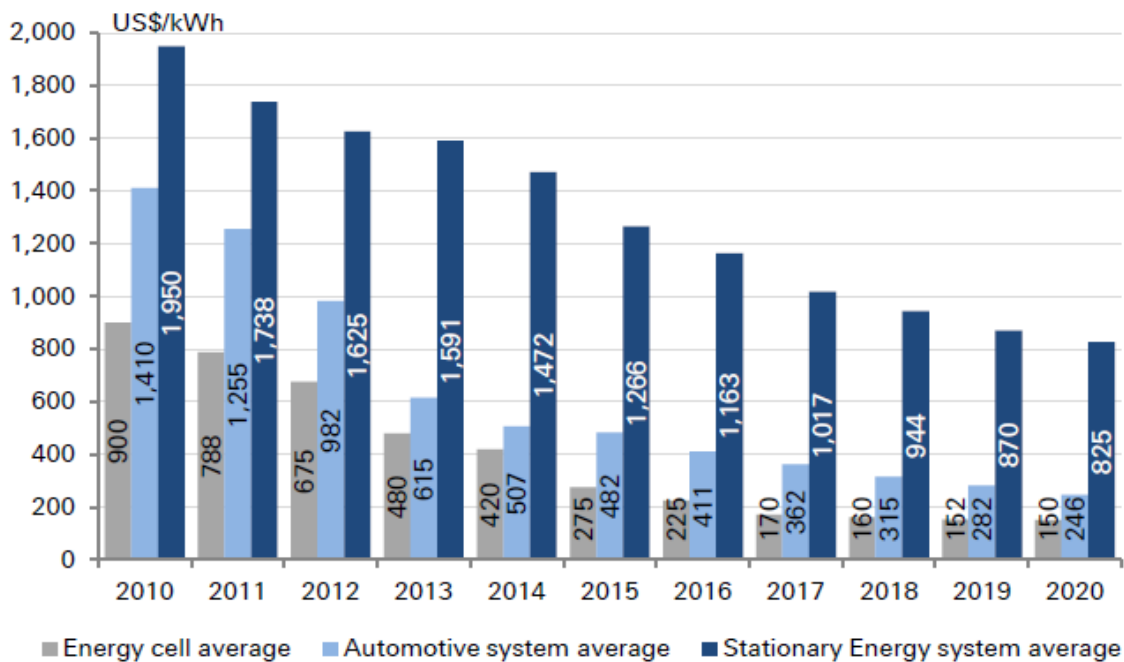*Figure 16: Forecasted battery pack prices for EVs. [44]*

Figure 17: Evolution of LIB cell and system cost for EV and stationary storage applications. [45]
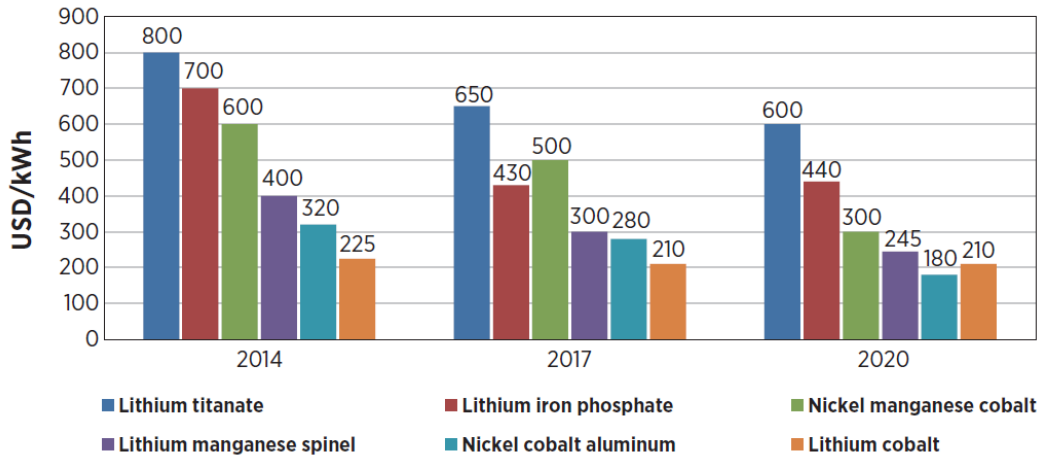
Figure 18: Cost estimates of different LIB technologies for grid storage applications. [38]

3.6   Modelling of battery storage systems

Battery characteristics are conventionally expressed in current/voltage/SOC (*I/U/SOC*) domain, in which electrical quantities and are used to model the system. Current is regarded as an input, and other quantities are then regarded as outputs. The SOC (Θ in Ah and θ in p.u. values), terminal voltage (U_b), terminal power (P_b), and SOE (Ψ) can be estimated by using electrical equivalent circuits:

$$\Theta(t) = \Theta(t-1) - \int I \; dt \tag{9}$$

$$\theta = \frac{\Theta}{Q_n} \tag{10}$$

$$U_b = U_{oc} - RI \tag{11}$$

$$P_b = I\left(U_{oc} - RI\right) \tag{12}$$

$$\Psi(t) = \Psi(t-1) - \int U_{oc} I \; dt \tag{13}$$

where the current was defined positive for discharge, which is typical for battery modelling, although opposite to the conventions used in power systems. Also power and energy losses and instantaneous efficiency can be calculated. The above equations represent the battery operation. This kind of modelling is accurate, but the model is complex and highly nonlinear. Moreover, for modelling of a complete ESS, the PCS needs to be modelled separately, which adds complexity.

In power systems, the level of abstraction is higher, and linear or piecewise-linear models are used to ensure high performance in numerical optimisation. The variables of interest are the applied power and the state of energy (SOE), i.e., *P/SOE* domain is used. Here, the applied power is regarded as an input, and the SOE is regarded as an output. However, because the terminal voltage, current, and internal resistance are not involved, the connection between the applied AC discharging or charging power (P_{dch} and P_{ch}) and the SOE (Ψ) is made through the efficiency:

$$\begin{cases} \Psi(t) = \Psi(t-1) - \int \dfrac{1}{\eta^{\text{dch}}} P^{\text{dch}} dt, \text{ for discharging} \\ \Psi(t) = \Psi(t-1) + \int \eta^{\text{ch}} P^{\text{ch}} dt, \text{ for charging} \end{cases} \tag{14}$$

$$\psi = \frac{\Psi}{E_{\text{n}}} \tag{15}$$

This efficiency is the total efficiency of the power conversion, i.e., it includes also the efficiency of the inverter. Examples of the efficiency characteristics were shown in Figure 13 and Figure 15. In general, a look-up table or a mathematical function in respect to the SOE and power can be used. However, these would result in a nonlinear model, which is undesirable. A linear model can be obtained by using piecewise-linear efficiency curve or a constant efficiency. As was discussed in Section 3.2 and illustrated in Figure 13 and Figure 15, the total efficiency curve is fairly flat for the most of the operating area. The use of constant efficiency will result in fairly high accuracy, if the low-efficiency regime at very low power can be avoided and low E-rates are used.

The relationship between the SOE and the SOC can be represented as

$$\Psi = \Theta \cdot U_{\text{oc}} \tag{16}$$

The OCV is a nonlinear function of the SOC, and hence, also the SOE is a nonlinear function of the SOC. As an illustration, the OCV vs SOC as well as the SOE vs SOC curves for a commercial Kokam 40-Ah NMC cell are shown in Figure 19. The OCV curve was obtained from [46]. The nonlinearity of the OCV curve is clearly seen at the inflection points at approximately 5% SOC and 65% SOC, where the slope changes significantly. Also the effect of cut-off voltages can be evaluated here. The cell datasheet specified 2.7 V as the minimum voltage and 4.2 V as the maximum voltage, while the module datasheet specified 3.0 V as the minimum voltage and 4.15 V as the maximum voltage. The nominal capacity was 40 Ah, while the measured capacity for the module-specified cut-off voltages was almost 43 Ah [46]. For grid storage applications, it is common to

specify a low cut-off voltage in the order of 3.2–3.3 V, which further narrows the voltage range, and consequently, reduces the useable energy. However, as a trade-off, it provides more stable voltage and likely a longer lifetime.
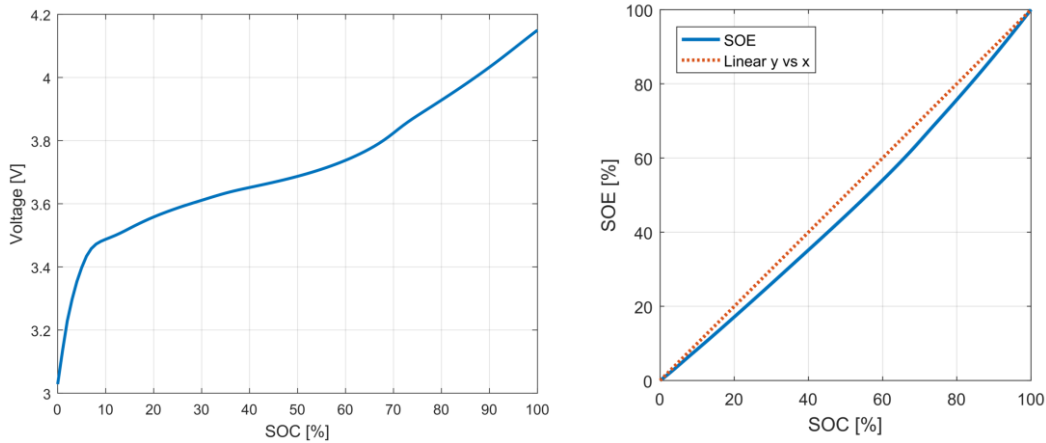

Figure 19. Interdependencies between OCV, SOC, and SOE for a commercial Kokam 40 Ah NMC cell. Left panel: OCV vs SOC. Right panel: SOE vs SOC. A linear curve was drawn to guide the eye.

3.7 Pilots' storage systems and duty cycles

Battery systems in the INVADE pilot sites are different and they are used in various applications. Brief descriptions of the pilots are given in [6]. The offered flexibility services are provided in [5], and some preliminary information about the storage requirements are gathered in [3].

Some basic information of each pilot site and their storages is presented in Table 5. Even though only the Norwegian pilot has decided the storage supplier, the preliminary choices indicate that two pilots will use similar second-life batteries of LMO–NMC technology and two pilots will use NMC technology. The P/E ratio is in the order of 1:1 for the Bulgarian, the Spanish, and the Netherlands pilots, and approximately 3:2 for the Norwegian pilot. These ratios are fairly low, but continuous use at a rate of 1C may result in moderate heating. Furthermore, the typical power levels will be lower than the rated power capacity. For example, the typical cycle for the Spanish pilot is 100 kW discharge for 30 min, which equals to approximately 25% cycle depth at a rate of C/2. These ratios are low, which ensures good electrical and thermal performance and long lifetime. Furthermore, the low ratios also minimise the effect of rate and temperature stressors.

Table 5. Applications and characteristics of the batteries used in the INVADE pilot sites.

Pilot	Application	Total capacity	Battery type
Bulgaria	Centralized battery for hotel and restaurant, connected to PVs.	200 kWh / 200 kW*	NMC*
Norway	30 residential batteries connected to PVs, EV-chargers and smart heating systems. One battery connected to PV and 11 smart EV-chargers.	30 x 4,2 kWh / 6 kW (residential)	LMO+NMC (Nissan 2nd life)
The Netherlands	Centralized battery next to an office building. Local balancing: solar panels, windmills, EV charging.	138 kWh / 140 kW*	NMC*
Spain	Backup battery storage system connected to the grid. Secures electricity supply for critical buildings. Can also be used to balance production and consumption in the area.	200 kWh / 200 kW* (100 kWh for backup, 100 kWh for balancing)	LMO+NMC* (Nissan 2nd life)
* Preliminary information, definitive selection and purchase process not yet concluded.			

4 Optimal operation and control of storages

4.1 Objective functions

The objective functions for the flexibility management controller algorithm for prosumers and distribution system operators (DSOs) were defined in [2] and [1]. These objective functions are described and represented in this section to illustrate the complexity of the optimization problem. Original notation is used in the equations of this section. As the notation used in the equations of [2] and [1] was totally different than the notation used in this report, the notation of this section is totally different than in rest of this report. The reader should refer to the original reports for the notation and for more details regarding the objective functions.

4.1.1 Prosumer objective function

The value of flexibility for prosumers is dependent on the tariff/contract setup, capacity limitation, cost for different types of flexibility and other parameters. For these reasons, the objective function for prosumers will vary from case to case, including from pilot to pilot, but also within pilots. However, in general terms, we can state that the objective is a cost minimization function, subject to a set of constraints, where some are technical and some more related to commercial/contractual terms.

For prosumers the objective is to minimize the total expected costs, consisting of costs for the electricity retail contract (energy related fee), electricity taxes, grid contract (energy and peak demand charge), and minus revenues from selling surplus electricity back to the grid. Finally, the costs for activating flexibility are included. This is formulated in Equation (17).

$$\min z = \sum_{t \in T} \left[\left(P_t^{\text{retail-buy}} + P_t^{\text{grid-buy}} + P_t^{\text{tax}} \right) \chi_t^{\text{buy}} P^{\text{VAT}} - \left(P_t^{\text{retail-sell}} + P_t^{\text{grid-sell}} \right) \chi_t^{\text{sell}} \right] \\ + P^{\text{peak}} \chi^{\text{peak}} P^{\text{VAT}} + \zeta^{\text{flexibility}} \tag{17}$$

This objective function includes the flexibility operator (FO) activation cost for executing flexibility and the minimization cost for prosumers during periods without DSO or balance responsible party (BRP) requests. Other prosumer's economic compensations like the availability fee should be considered in the settlement process but they are not included in the operation phase.

Furthermore, the objective function reflects the total cost per period (t) that a prosumer has during each scenario. Scenarios represent a possible realization of the uncertain parameters.

The objective function can be different in each country or even region according to the electricity tariff structure. According to D4.1 *Overall INVADE architecture* [4], the prosumer services covered in this document are defined as:

ToU optimization is based on load shifting from high-price intervals to low-price intervals or even complete load shedding during periods with high prices. This optimization requires that tariff schedules are known in advance (e.g., day-ahead) and will lower the Prosumer's energy bill.

kWmax control is based on reducing the maximum load (peak shaving) that the prosumer consumes within a predefined duration (e.g., month, year), either through load shifting or shedding. Current tariff schemes, especially for commercial and industrial (C&I) customers, often include a tariff component that is based on the prosumer's maximum load (kWmax). By reducing this maximum load, the prosumer can save on tariff costs. For the DSO, this kWmax component is a rudimentary form of demand-side management.

Self-balancing is typical for prosumers who also generate electricity, e.g., through solar photovoltaic (PV) or combined heat and power (CHP) systems. Value is created through the difference in the prices of buying, generating, and selling electricity (including taxation if applicable). Note that solar PV self-balancing is not meaningful where national regulations allow for administrative balancing of net load and net generation.

4.1.2   DSO objective function

The DSO objective function is a service that will be utilized in the Spanish pilot. DSO flexibility mainly refers to avoiding thermal overload of system components by reducing peak loads where failure due to overloading may occur. This is seen as an alternative approach to installation of larger, more expensive transformers and cables. When a DSO requests flexibility, the FO delivers the requested flexibility by a portfolio of prosumers with flexible resources. By assessing the cost and availability of the different resources in the flexibility portfolio, the FO schedules and activates the resources correspondingly. The objective functions for the DSO and the FO are shown in Equations (18) and (19), respectively. They are further discussed in D5.3 [1].

$$F_t = \sum_{b \in B} \left(\sigma_{b,t}^{dch} - \sigma_{b,t}^{ch} \right) + \sum_{g \in G} \left(\psi_{g,t} - W_{g,t}^{prod} \right) + \sum_{l \in G} W_{l,t}^{load} \left(\delta_{l,t}^{start} - \delta_{l,t}^{run} \right)$$
$$+ \sum_{L^p} \left(W_{l,t}^{load} - \omega_{l,t} \right) + \sum_{L^y} \left(W_{l,t}^{load} - \omega_{l,t} \right) + \sum_{v \in V^s} \left(W_{v,t}^{EV} - \varphi_{v,t}^{ch} \right) + \sum_{v \in V^c} \left(W_{v,t}^{EV} - \omega_{l,t}^{CD} \right) \tag{18}$$

$$\min z = \sum_{t \in T} \left(\sum_{g \in G} P_{g,t}^{G} \left(W_{g,t}^{prod} - \psi_{g,t} \right) + \sum_{b \in B} P_{b,t}^{B,ch} \sigma_{b,t}^{ch} + P_{b,t}^{B,dch} \sigma_{b,t}^{dch} + \sum_{l \in L^c} P_{l,t}^{load} \left(\delta_{l,t}^{start} + \delta_{l,t}^{run} \right) \right)$$
$$+ \sum_{l \in L^c} \sum_{i \in I} P_l^s \psi_{l,i} + \sum_{v \in V^c} \left(\sum_{t \in T} \left(P_{v,t}^{EV} \frac{W_{v,t}^{EV} - \sigma_{v,t}^{CD}}{O_v^{CD}} \right) + P_v^{EV,NS} \left(O_v^{CD} - \sigma_{v,T_v^{EV,end}}^{CD} \right) \right) \tag{19}$$

In a case where the forecasted demand in a local distribution grid is higher than what the local cable or transformer can handle, a pre-charged battery can discharge and provide power in the local node. The battery has to be placed on the other side of the critical component in order to solve the problem. As batteries are always available, they provide stable, valuable flexibility to the FO.

4.2 Modelling of storage systems

4.2.1 State of energy

The SOE is dictated by the cumulative net energy of the battery, i.e, the difference between the charged and discharged energy, and it needs to stay within the specified minimum (Ψ_{min}) and maximum (Ψ_{max}) limits:

$$\Psi(t) = \Psi(t-1) + T_s \left[\sigma^{ch}(t) \cdot \eta^{ch} - \frac{\sigma^{dch}(t)}{\eta^{dch}} \right] \tag{20}$$

$$\Psi_{min} \leq \Psi(t) \leq \Psi_{max} \tag{21}$$

where Ψ is the SOE, T_s is the time step, σ^{ch} is the charging power, σ^{dch} is the dischaging power, η^{ch} is the total ESS efficiency during charging, and σ^{dch} is the total ESS efficiency during discharging.

Upper bounds for charging and discharging power are defined as

$$\begin{cases} \sigma^{dch} \leq V(t) P^{dch} \\ \sigma^{ch} \leq \left(1 - V(t) \right) P^{ch} \end{cases} \tag{22}$$

where P^{ch} and P^{dch} are the power constraints regarding charging and discharging, respectively, and the variable $V(t)$ is a binary variable which ensures that charging and

discharging cannot take place during the same time step. This can happen if charging and discharging are either zero or limited to a specific range between lower and upper bounds. This kind of constraint is relevant due to the fact that the inverter efficiency decreases rapidly at low power levels and in practise these low charging or discharging are never applied. If the time step is long enough (like one hour), then this constraint is hardly needed as the low power level can be interpreted as an average value over the whole time step and simultaneous charging and discharging will not appear. The power constraints will be addressed in more detail in Section 4.2.7.

All the equations above are applicable for any storage process, like a hot water heat storage. What makes battery storages different is the nature of ageing of the storage caused by the way charging and discharging are carried out. This degradation is a real cost of the use of the battery storage and it has to be taken into account in designing the operational policy and calculating the costs of the storage. The cost of degradation is addressed in Section 4.3.

4.2.2   Energy capacity

Constant energy capacity will be used in the model. That is, the rate effect and the temperature effect will not be taken into account.

4.2.3   Maximum charge and discharge power

Continuous power ratings will be used in the model, i.e., peak-power operation is not modelled. The power variable represents the average power during a time step.

4.2.4   Efficiency

A constant efficiency will be used in the first phase. The use of constant efficiency is expected to cause only a small modelling error in most cases. However, in case of high share of operation in the low-efficiency regime of the PCS is expected, a piecewise linear model may be adapted to improve the accuracy.

4.2.5   Self-discharge

Self-discharge is not taken into account in the model, because LIBs have very low self-discharge rates. Self-discharge characteristics are in the order of few percent in a month. Typical characteristics for different chemistries were shown in Table 1. These rates are insignificant from the point-of-view of modelling.

4.2.6   Performance degradation due to ageing

The useable energy capacity is impacted by the performance degradation due to ageing. The time-scale of ageing is much longer than the prediction horizon of the optimisation algorithm. Therefore, the energy-capacity parameter can be a constant. However, the parameter needs to be adapted once in a while to the measured or estimated capacity. In case diagnostic capacity check-up tests are being performed periodically, as was proposed in D6.3 [7] for centralised storages, the parameter shall be adapted to the measured value after each check-up test, which is performed approximately once in a month. For distributed storages at homes, a linear relationship between cumulative discharged energy and the SOH shall be assumed.

The energy efficiency may be impacted by the performance degradation due to ageing. However, this effect is not taken into account in the model.

4.2.7   Limitations and constraints of operation

Manufacturer-specified limits regarding current, voltage, and temperature should not be violated in any case. The BMS monitors these values and reduces maximum charging and discharging current in case these limits are approached. As a consequence, tapering of current is activated when a battery approaches fully-charged or fully-discharged state, and when the operating temperature is high or low. When approaching fully-charged state, tapering of current is initiated when the highest-voltage cell reaches the specified maximum voltage. The current is then tapered to avoid the voltage to exceed the specified maximum cell voltage until a cut-off current is reached. When approaching low cut-off voltage, the tapering is initiated when the lowest-voltage cell reaches the specified minimum voltage. The current is then tapered to avoid the voltage to exceed the specified minimum cell voltage until a cut-off current is reached. However, all BMSs or EMSs do not have this kind of tapering implemented when approaching fully-discharged state. Instead, they may abruptly interrupt the current to zero when the minimum voltage is reached.

During charging, the boundary between the normal operation and the voltage-limited operation depends on the rate, the internal impedance, and the OCV characteristics. Typical SOC values for the boundary at C/3, 1C, and 2C rates are 95%, 90%, 80%. However, these numbers vary and depend especially on the cell chemistry. During discharging, the actual boundary between the constant-current or constant-power operation and the current-tapered or voltage cut-off operation is typically close to 0% SOC for discharging with rates of less than 3C. Nevertheless, the power limiting region

should start at around 10% SOC to prevent abrupt ending of the discharge due to accidentally reaching the cutoff voltage. Also the efficiency starts to reduce significantly already before that, and the heat generation rate increases rapidly as the SOC approaches 0%.

For full utilization of the battery performance without voltage-based limitations, a SOE range that allows full-power operation can be defined. Moreover, this region can be further reduced in order to take into account other aspects such as increased rate of aging at high SOE and lower efficiency at low SOE.

Different charging and discharging power constraints can be used to avoid unfavourable operating points. Linear charging and discharging power constraints can be used to implement tapering due to the need to strictly avoid exceeding the specified maximum cell voltage during charging and to avoid abrupt ending of discharge due to exceeding the specified minimum cell voltage during discharging, respectively. Moreover, the detrimental effects caused by high-rate charging at high cell voltage are reduced too. However, the linear constraint works optimally only for very short time steps, for which the SOE cannot change much during a time step. For longer time steps, another linear constraint needs to be defined: maximum average power for a given time step. This constraint defines the power that fully charges or discharges the storage up to the defined maximum or minimum SOE during a time step, respectively. The applied power is also limited by the manufacturer-specified rated discharging power and rated charging power. Additionally, minimum SOE and maximum SOE may be constrained to avoid certain operating points, which might, e.g., be detrimental to the lifetime.

Constraint to avoid current tapering:

$$P^{\text{ch}} \leq \frac{P_{\text{r}}^{\text{ch}}}{1 - \psi_{\text{b-r}}^{\text{ch}}} \left(1 - \psi\right) \tag{23}$$

$$P^{\text{dch}} \leq \frac{P_{\text{r}}^{\text{dch}}}{1 - \psi_{\text{b-r}}^{\text{dch}}} \cdot \psi \tag{24}$$

Constraint to limit average power due to long time step:

$$P^{\text{ch}} \leq \frac{E_{\text{r}}}{T_{\text{s}}} \left(1 - \psi\right) \tag{25}$$

$$P^{\text{dch}} \leq \frac{E_{\text{r}}}{T_{\text{s}}} \cdot \psi \tag{26}$$

In addition to constraints on the maximum charging and discharging power, a constraint on the minimum power during operation can be defined as well to avoid operation in the low-efficiency regime of the inverter. In this case, there is a minimum power threshold that prevents charging or discharging at a lower power than the threshold power. If the power reaches the threshold power, the charging or discharging is terminated.

The different constraints regarding the maximum charging power are illustrated in Figure 20 for an ES system specified with an E-rate of 1E, a maximum SOE of 95%, and a time step of 15 min. The total constrained charging power regime is the area within these limits and constraints. The time step has a high impact on the slope of the maximum average power during a time step. The full-power regime is reduced as the time step is increased. For 15-min time step and 95% maximum SOE, the power of a 1E-rated storage needs to be reduced when exceeding approximately 75% SOE. In a similar manner, the different constraints regarding the maximum discharging power are illustrated in Figure 21 for an ES system specified with an E-rate of 1E, a maximum SOE of 95%, and a time step of 15 min.

Figure 20: Charging power constraints (rated power, constant-power mode, time-step, minimum power, maximum SOE) for an ESS specified with an E-rate of 1E, a maximum SOE of 95%, and a time step of 15 min. The shaded area shows the total applicable charging power regime.
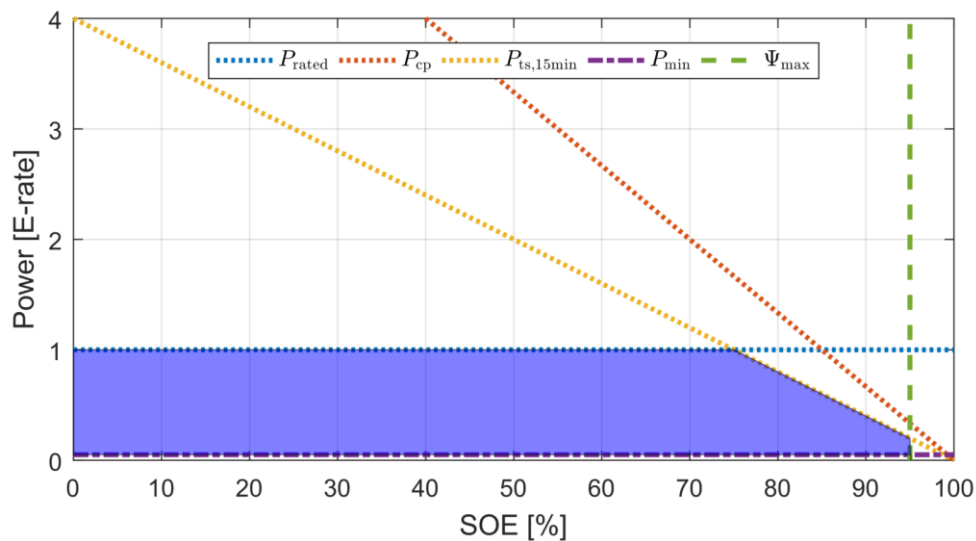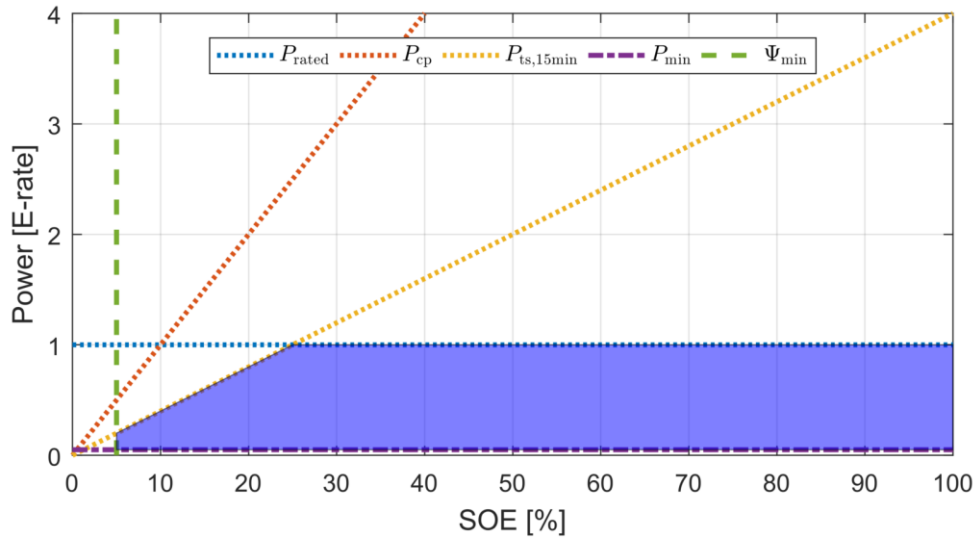
Figure 21: Discharging power constraints (rated power, constant-power mode, time-step, minimum power, maximum SOE) for an ESS specified with an E-rate of 1E, a maximum SOE of 95%, and a time step of 15 min. The shaded area shows the total applicable discharging power regime.

4.3   Cost of degradation

Battery operators must be able to submit bids that the marginal operating costs of the ESS. These marginal costs should include all the variable cost factors, also the cost of battery degradation caused by each cycle. The methodology described in [47] is adopted as a baseline. The cycle depth (∆DOD) has a substantial impact on the total attainable number of cycles. A model for the typical cycle lifetime vs ∆DOD characteristics from the literature were developed in Section 2.3 and presented in Figure 10 and Equation (8). In Figure 22, that model is adopted into a case in which the 100% cycle depth corresponds to 1000 cycles.
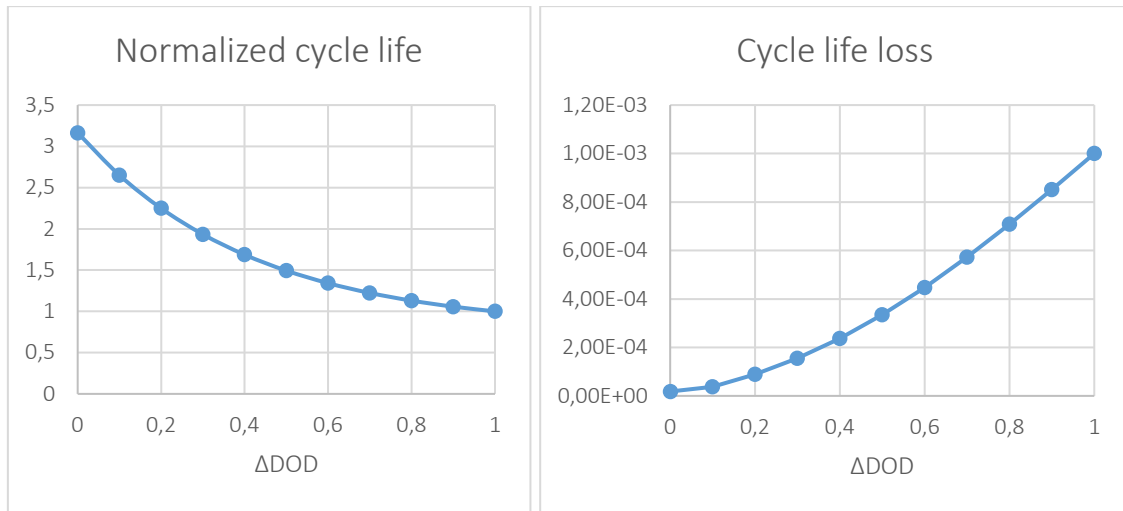
Figure 22. Normalized cycle life and the corresponding cycle life loss.

With a cycle starting from a full charge towards the depth of 20% and then back, the maximum number of cycles is about 11,245 (assuming that 1000 cycles is the maximum amount of cycles having 100% depth). That is, a cycle with ΔDOD (or $\Delta\delta$) of 20% uses one cycle of out the total of the above mentioned 11,245. This means that every cycle from 100% to 80% SOE consumes $1/11{,}245 = 0.000089$ ($8.89*10^{-5}$) or 0.009% of the total life. If the investment cost of a battery per storage volume is 1000 €/kWh, then the cost of one 20% DOD cycle is 1000 €/kWh$*1/11{,}245 = 0.09$ €/kWh.

If we denote the battery investment cost by K, the rated capacity of the storage by E_n and the discharge efficiency by η^{dch}, then we can write a specific investment cost (c_0) for a battery storage as follows:

$$c_0 = \frac{K}{\eta^{dch} E_n} \tag{27}$$

By defining the battery cycle loss function $\Phi(\Delta\delta)$ this cost function can be modified into degradation unit cost function, as follows:

$$c = \frac{K}{\eta^{dch} E_n} \Phi(\Delta\delta) = C_b \cdot \Phi(\Delta\delta) \tag{28}$$

where C_b is the replacement cost of the battery.

We describe two alternative approaches that has been used in the literature. The first one, the direct linearization (as we call it here), is based on using the degradation cost curve (i.e., specific investment cost times the cycle life loss function) directly in defining the cost. In this method the battery is handled as one unit and the nonlinear degradation

cost curve is linearized in piece by piece. The second method is based on the well-known rainflow algorithm that has its use in material fatigue analysis. In this method, the battery is divided into evenly sized segments. Each segment corresponds to a specific cycle depth having specific marginal degradation cost. This is obtained as a derivative of the linearized degradation cost. The cost of degradation is then calculated as marginal cost multiplied by activity level (discharge) in each segment and the total cost is obtained by summing up over the segments. So, both of the methods use the same input data, but they use it in alternative ways. In what follows, we define these methods in a detailed enough level and then compare the results obtained by the methods we have implemented in GAMS.

4.3.1   Direct linearization

The cost of degradation based on the cycle depth is a nonlinear function. Figure 22 illustrates a ten-segment linearization of one example of such a curve, where the depth of discharge, delta, is defined as $\delta_t = \delta(t) - \delta(t-1)$. During charging, this expression gives negative values that are excluded, i.e., only the positive values refer to discharging and we allocate all the costs of degradation on discharging.

For a battery, the points of the piecewise linear approximation are given by their coordinates, $(\Delta\delta, \Phi(\Delta\delta))$. For any $\Delta\delta$ we can find the corresponding $\Phi(\Delta\delta)$ by using a linear interpolation between the points of the piecewise linear approximation with the help of the following set of equations using special order sets of type 2 (SOS2) [48]:

$$\sum_{j \in J} x_j \cdot L_{t,j} = \Delta\delta_t \tag{29}$$

$$\sum_{j \in J} y_j \cdot L_{t,j} = \Phi(\Delta\delta_t) \tag{30}$$

$$\sum_{j \in J} L_{t,j} = 1$$
$$\text{where } L_{t,j} \in SOS2 \tag{31}$$

At most two variables within a SOS2 can have non-zero values. The two non-zero values have to be adjacent. The most common use of SOS2, and the one applied here, is to model piecewise linear approximations to nonlinear functions.

The difference in DOD (or SOE) in consecutive steps defines the value of the x-axis variable and $C_b \cdot \Phi(\Delta\delta)$ gives the corresponding cost. In other words, in each time step

the change in DOD (x-axis value) is measured, its position is defined using the segments, and the corresponding cost is determined on the y-axis.

Total cost of degradation over the planning period can now be defined as

$$C_{\text{deg}} = \sum_t c_t \tag{32}$$

This is part of the objective function that will be defined below.

This method has no sense of history: it focuses entirely on the change from the previous state to the present state. The easiest way to improve the method is to take into account also the (possible) discharge in the previous step by simply adding it to right hand side of the Equation (29): $\Delta\delta_t \rightarrow \Delta\delta_t + \Delta\delta_{t-1}$. This addition is capable of noticing discharge on two consecutive steps—a small improvement over one step process. The degradation cost function looks now as follows:

$$c_t = C_b \Phi(\Delta\delta_t + \Delta\delta_{t-1}) \tag{33}$$

4.3.2 Segmenting the cycle depth

The rainflow counting algorithm, which is extensively used in materials stress analysis to quantify the cumulative impact of cycles, can also be used in battery life assessment [47]. The rainflow method [47] identifies cycles when a SOE profile with a series of local extrema (i.e. points where the current direction changed) is given: s_0, s_1, …, etc.
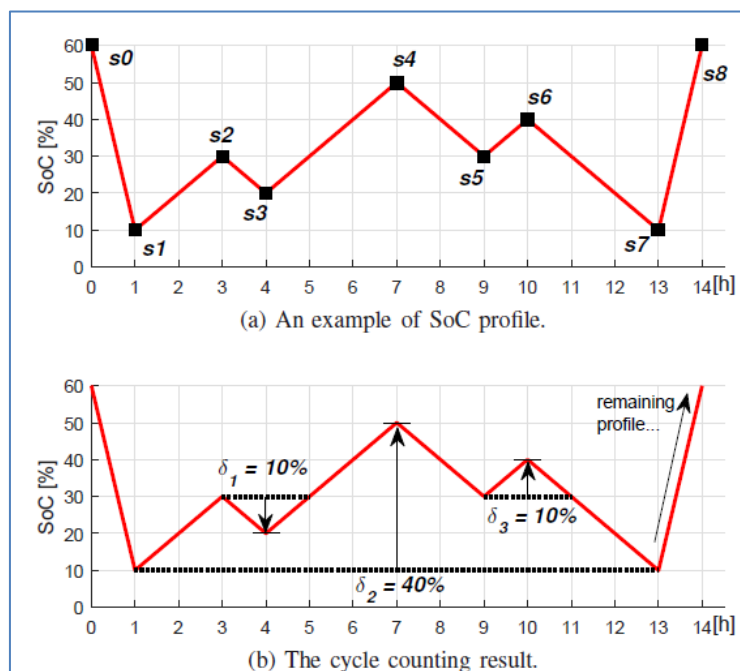

Figure 23. Using the rainflow algorithm to identify battery cycle depths. [47]

The algorithm advances as follows:

1. Start from the beginning of the profile (as in Figure 23(a)).

2. Calculate $\Delta s_1 = |s_0 - s_1|$, $\Delta s_2 = |s_1 - s_2|$, $\Delta s_3 = |s_3 - s_2|$

3. If $\Delta s_2 \leq \Delta s_1$ and $\Delta s_2 \leq \Delta s_3$, a full cycle of depth Δs_2 associated with s_1 and s_2 has been identified. Remove s_2 and s_3 from the profile and repeat the identification using points s_0, s_1, s_4, $s_5, \ldots$

4. If a cycle has not been identified, shift the identification forward and repeat the identification using points s_1, s_2, s_3, $s_4, \ldots$

The identification is repeated until no more full cycles can be identified throughout the profile.

The remainder of the profile is called the rainflow residue and it contains only half cycles. A half cycle with decreasing SOE is a discharging half cycle, while a half cycle with increasing SOE is a charging half cycle. For example, the SOE profile shown on Figure 23(b) has two full cycles of depth 10% and one full cycle of depth 40%, as well as a discharging half cycle of depth 50% and charging half cycle of depth 50%.

The rainflow algorithm cannot be integrated directly within an optimization problem, but following the method described in [47] to implement the rainflow counting algorithm makes it possible to use it in an optimization model. In this model the total life lost *L* from a SOE profile is assumed to be the sum of the life loss over all the number of cycles identified by the rainflow algorithm.

The formulation of the rainflow method implementable into an optimization model thus divides the battery into *J* segments and keeps them separate. They are interconnected only by summation. Each segment has for each time step the SOE, the charging power, and the discharging power variables. The advantage obtained by this formulation is to avoid using the SOS variables needed to keep track of the change in the SOE and the degradation cost related to the change.

The equations describing the battery dynamics are now the following:

$$P_t^{\mathrm{dch}} = \sum_{j=1}^{J} p_{t,j}^{\mathrm{dch}}$$
$$P_t^{\mathrm{ch}} = \sum_{j=1}^{J} p_{t,j}^{\mathrm{ch}} \tag{34}$$

$$P_t^{\mathrm{dch}} \leq P_{\max}^{\mathrm{dch}} \cdot V_t$$
$$P_t^{\mathrm{ch}} \leq P_{\max}^{\mathrm{ch}} \cdot \left(1 - V_t\right) \tag{35}$$

$$e_{t,j} - e_{t-1,j} = T_\mathrm{s}\left(\eta^\mathrm{ch} p_{t,j}^\mathrm{ch} - \frac{1}{\eta^\mathrm{dch}} p_{t,j}^\mathrm{dch} \right) \tag{36}$$

$$e_{1,j} = e_j^0$$
$$e_{t,j} \leq e_j^\mathrm{max} \tag{37}$$

$$E^\mathrm{min} \leq \sum_{j=1}^{J} e_{t,j} \leq E^\mathrm{max} \tag{38}$$

$$\sum_{j=1}^{J} e_{t,j} \geq E^\mathrm{final} \tag{39}$$

V is a binary variable that prevents simultaneous charging and discharging.

When discharging the energy content of the battery develops as (assuming 60-min time step and moving into relative values by dividing both sides by the rated capacity E_n):

$$\frac{e_{t,j} - e_{t-1,j}}{e_\mathrm{n}} = \frac{T_\mathrm{s}}{\eta^\mathrm{dch} e_\mathrm{n}} P_{t,j}^\mathrm{dch}$$
$$\Leftrightarrow \Delta\delta_t = \frac{T_\mathrm{s}}{\eta^\mathrm{dch} e_\mathrm{n}} P_{t,j}^\mathrm{dch} \tag{40}$$

The incremental ageing from this cycle is $\Phi(\Delta\delta)$. The marginal ageing is obtained by taking a derivative with respect to discharging power

$$\frac{\partial \Phi(\delta)}{\partial P^\mathrm{dch}} = \frac{d\Phi(\Delta\delta)}{d\delta} \cdot \frac{\partial \delta}{\partial P^\mathrm{dch}} = \frac{T_\mathrm{s}}{\eta^\mathrm{dch} e_\mathrm{n}} \cdot \frac{d\Phi(\Delta\delta)}{d\delta} \tag{41}$$

To define the marginal cost of ageing we include the battery replacement cost C_b into the marginal cycle ageing and construct a piecewise linear approximation function *c*. This function consists of *J* segments that evenly divide the cycle depth range from 0 to 100 %. For each segment:

$$\frac{d\Phi(\Delta\delta)}{d\delta} \rightarrow \frac{\Delta\Phi(\Delta\delta)}{\Delta\delta} = \frac{\Phi\left(\frac{j}{J}\right) - \Phi\left(\frac{j-1}{J}\right)}{1/J} = J \cdot \left[\Phi\left(\frac{j}{J}\right) - \Phi\left(\frac{j-1}{J}\right) \right] \tag{42}$$

The degradation cost for each segment using the battery investment cost *K* can now be defined as

$$c_j = K \cdot \frac{1}{\eta^\mathrm{dch} E_\mathrm{n}} \cdot \frac{\left[\Phi\left(\frac{j}{J}\right) - \Phi\left(\frac{j-1}{J}\right) \right]}{1/J} = C_\mathrm{b} \cdot J \cdot \left[\Phi\left(\frac{j}{J}\right) - \Phi\left(\frac{j-1}{J}\right) \right] \tag{43}$$

The cost differences of the adjacent segments form the core of the definition. Defining the cycle aging cost function as $\Phi(\Delta\delta)=100(\Delta\delta)^2$ ($\Phi(\delta)=\{0,1,4,9,16,\ldots,100\}$), the cost vector obtained is then $c_j=\{1,3,5,7,9,11,13,15,17,19\}$.

The cycle ageing cost is a sum of the cycle aging costs associated with each segment over the horizon:

$$C_{\deg} = \sum_{t,j} c_j \cdot \left(T_s \cdot p_{t,j}^{\mathrm{dch}}\right) \tag{44}$$

The term in the brackets defines the amount of energy discharged.

4.3.3   Comparing the modelling approaches

Figure 24 compares the rainflow algorithm, the optimization compatible rainflow method [47] and the degradation cost linearization method [48]. We use the same cycle aging cost function as above: $\Phi(\Delta\delta)=100(\Delta\delta)^2$. Both the OptRain and the rainflow methods end up in the same degradation costs but the routes used to calculate it differ. The basic linearization method LinearZ takes into account only the change in the DOD and interprets it as cycle depth when defining the cost. This leads to lower costs of degradation because the deeper cycles are left unnoticed. The slightly advanced method LinearZ_2 looks one step backward and the results improve: The costs in this example exceed those of the rainflow based methods. The smaller costs of the LinearZ method anticipate large variations for the state of energy of the battery in the simulations. The rainflow methods are capable of identifying larger cycles which leads to higher and more realistic cost estimates, as seen in steps 9, 12 and 13 in the OptRF line and the 40% cycle cost of 16 units in the original RainFlow method.

Notice that the energy segments at the top table are not all the time populated from bottom to the top. The cost of discharge is smallest for the first (shallowest) segment so it is discharged—and charged—at first. To get energy back from the deeper segments is possible only by using larger cycle depth at higher cost. The algorithm keeps the charged energy in its original segment until it is actually discharged at a cost corresponding with its depth.

Time step		0	1	2	3	4	5	6	7	8	9	10	11	12	13	14
Storage	SoE, %															
segments	10	1	0	1	1	0	1	1	1	0	0	1	0	0	0	1
	20	1	0	0	1	1	1	1	1	1	0	0	0	0	0	1
	30	1	0	0	0	0	0	1	1	1	1	1	1	0	0	1
	40	1	0	0	0	0	0	0	1	1	1	1	1	1	0	1
	50	1	0	0	0	0	0	0	0	0	0	0	0	0	0	1
	60	1	1	1	1	1	1	1	1	1	1	1	1	1	1	1
	SoE, %	60	10	20	30	20	30	40	50	40	30	40	30	20	10	60
Discharge	Costs															
SoE[%] 10	1	0	1	0	0	1	0	0	0	1	0	0	1	0	0	0
20	3	0	1	0	0	0	0	0	0	0	1	0	0	0	0	0
30	5	0	1	0	0	0	0	0	0	0	0	0	0	1	0	0
40	7	0	1	0	0	0	0	0	0	0	0	0	0	0	1	0
50	9	0	1	0	0	0	0	0	0	0	0	0	0	0	0	0
60	11	0	0	0	0	0	0	0	0	0	0	0	0	0	0	0
OptRF	**43**	0	25	0	0	1	0	0	0	1	3	0	1	5	7	0
RainFlow	2				1						1					
	16			16												
43	25		25													
delta_DoD			50	10	10	10	10	10	10	10	10	10	10	10	10	50
rho	100d^2		25	1	1	1	1	1	1	1	1	1	1	1	1	25
LinearZ	**31**		25				1			1	1		1	1	1	
LinearZ_2	40		25				1			1	4		1	4	4	

Figure 24. Battery operation example (referring to Figure 23). Using the rainflow algorithm to identify battery cycle depths. Storage: energy by segment; Discharge: discharge by segment; OptRain: costs of discharge by segment; rainflow: costs of identified cycles; LinearZ: Degradation cost function linearization method (only discharging generates costs); LinearZ_2: Consecutive DOD summed up before cost calculation.

4.3.4 System definition for the experiments

In this section we show some properties of the models defined above and compare alternative formulations using the system shown in Figure 25. The load, or demand $L(t)$, is given and the battery is used to minimize energy procurement costs consisting of energy and peak power costs. In the experiments below we study system behaviour in two basic modes of battery use. In addition, we compare alternative battery model versions in several dimensions. All calculations are carried out with 15-min time step (exceptions are mentioned) which will likely be the applied time step in the electricity markets in future. The price and load development over one day is illustrated in Figure 26. Battery characteristics are the ones shown in Figure 22. The SOE and ∆DOD curves are approximated by 10 segments; $J = \{1, \ldots ,10\}$.
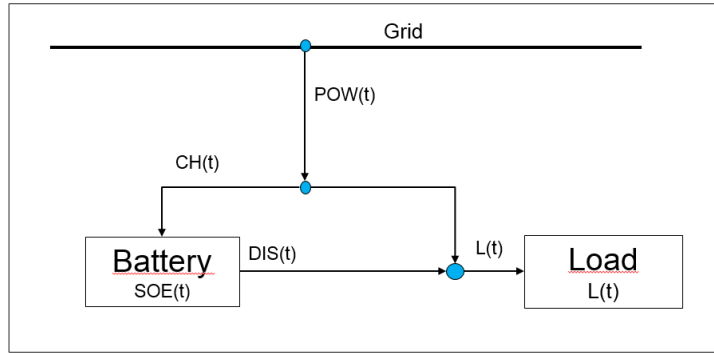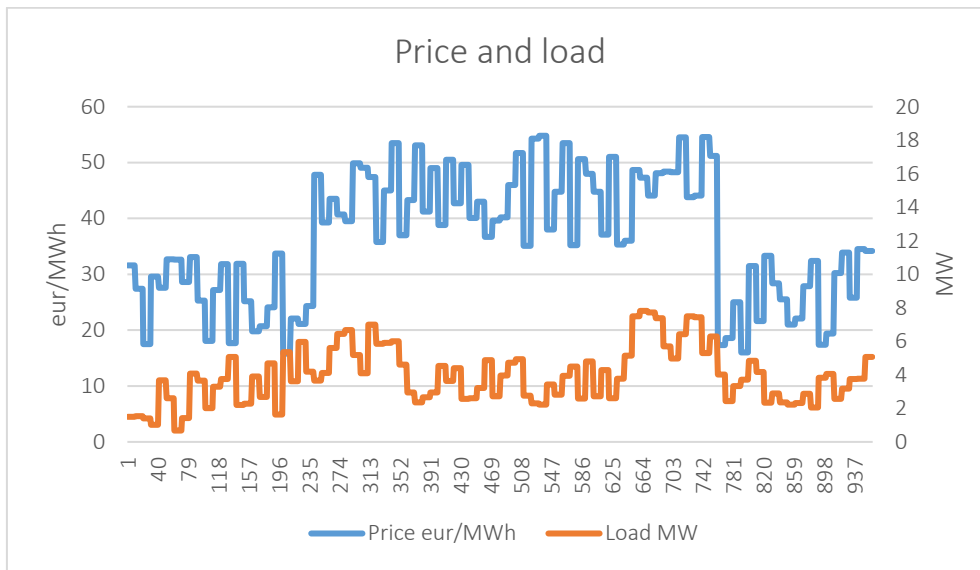
Figure 25. System setup for model experiments.

Figure 26: Electricity price and load. The 24-hour planning horizon is broken down into 15-min time steps.

4.3.5 Experiments with objective functions

We compare the model outcomes with three alternative objective functions. The first describes pure price arbitrage, i.e. trading energy for profit, without degradation costs, the second is the same with degradation costs included and the last one adds still one component: the peak power cost factor:

$$\max \left\{ \sum_t p(t) \cdot T_s \cdot \left(P_t^{\text{dch}} - P_t^{\text{ch}} \right) \right\} \tag{45}$$

$$\max \left\{ \sum_t p(t) \cdot T_s \cdot \left(P_t^{\text{dch}} - P_t^{\text{ch}} \right) - C_{\text{deg}} \right\} \tag{46}$$

$$\max \left\{ \sum_t p(t) \cdot T_s \cdot \left(P_t^{\text{dch}} - P_t^{\text{ch}} \right) - C_{\text{deg}} - P_{\text{px}} C_{\text{px}} \right\} \tag{47}$$

P_{px} is the peak demand over the period and C_{px} is the corresponding peak power cost per power unit. There are now three components in the objective function: minimizing both energy procurement costs and peak power cost and taking the degradation costs into account. Peak demand is defined as the highest power a customer takes from the grid during the planning period:

$$P_{px} \geq P_t^{ch} - P_t^{dch} + d_t \qquad (48)$$

where d_t defines the time-dependent demand of the battery owner. By timing the discharge it is possible to drive the peak demand down.

We have nine cases to compare: three modelling methods and three objective functions, which are all shown in Figure 27. The energy trading case without degradation costs (left panel) shows that the battery use is substantial and the model outcomes are the same for all the degradation cost modelling approaches—naturally as the approaches differ only in degradation costs are included in the cost definition. In the middle panel we include the degradation costs to the energy trading case. Clearly they make energy trading non-profitable as the battery stays idle all the time—no matter how the degradation costs are implemented. The right hand panel shows the impact of the peak power cost on the battery use economics: The battery comes active again to take care of peak load shaving. The OptRain method causes less ramping in the battery SOE compared to those of the Linearization cases. The SoE in LinZ2 ramps less than LinZ by taking the two last ΔDODs into account simultaneously.
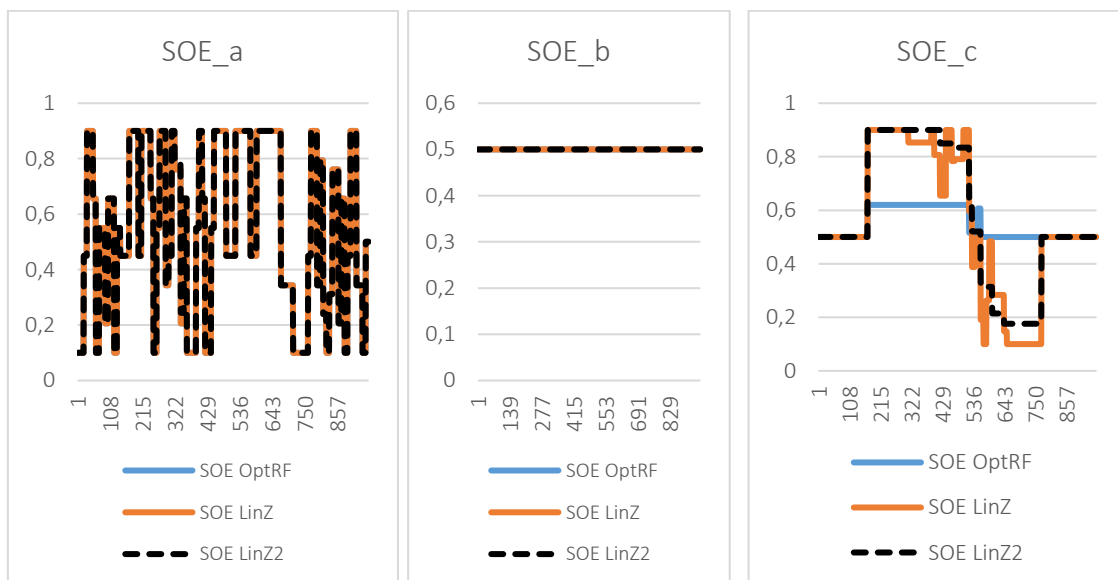

Figure 27: Left panel: without degradation cost; middle panel: degradation cost included; right panel: degradation costs and peak power costs included. (X-axis describes time: 96 15-min steps and 10 samples in each step = 960 samples in all.)
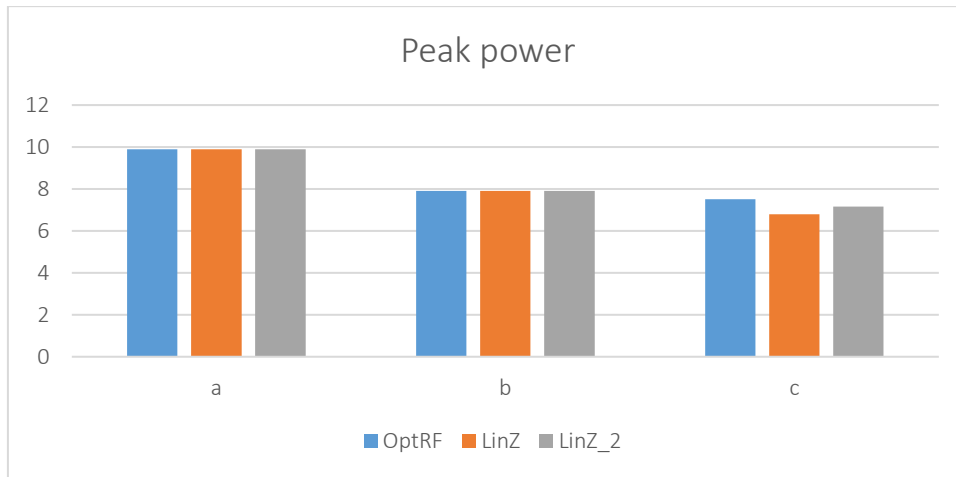
Figure 28. Peak power in the test cases. The letters a, b, and c refer to Equations (45), (46), and (47), *respectively, and peak power is defined in Equation* (48).

Power in case (*a*) is higher than in case (*b*) due to the fact that peak power has no cost and high load and battery charging takes place simultaneously: the use of the battery increases peak power but it can be done without extra cost. In this case only energy trading generates revenues and costs. In case (*c*) the peak power is highest in OptRF case, as it is the only one of the approaches capable of taking the degradation into account in a realistic manner. The linearization approaches are limited to the short term events only.

As an example, Figure 29 shows the battery usage with the original load, battery operations and the resulting peak power for case OptRF. The battery is used for peak shaving only—energy arbitrage is not economic with the price differences and degradation costs applied.
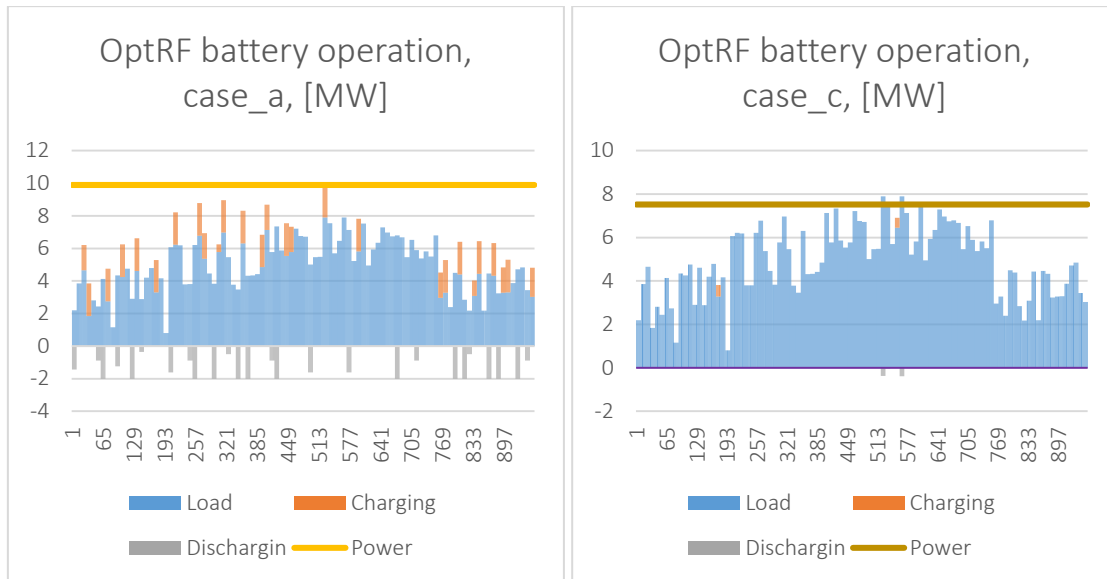
Figure 29. Timing of battery operations. Left panel: Without degradation costs and peak power cost. Right panel: Peak shaving when peak power has a cost and degradation costs included. The horizontal line describes the peak power after shaving.

4.3.6   Experimenting with the number of customers

In all the above results are based on a single user case with 24 hours of planning horizon. If we change our perspective from an individual customer to an aggregator or distribution network operator then the optimization problem is modified from a single user case into a multi battery system with possibly hundreds of batteries to be optimized. The way the problem is set up may have a dramatic impact on the time it takes to optimize the overall system.

Next we shall compare the solution times of the two modelling approaches in a system consisting of 30 batteries. The linearization approach uses 10 segment piecewise linearization as in all the above examples and the OptRF approach continues to use a 10 segment description of the battery storage.

The approximate sizes of the problems are as follows: OptRF: 34,600 rows and 80,350 columns; LinearZ and LinearZ_2 both has about 17,200 rows and 45,800 columns. The OptRF is about two to three times the size of the LinearZ problem due to the segmentation of the battery.

The execution times for one day (24 hours in 15-min steps) are the following: OptRF: 2.3 sec and LinearZ and LinearZ_2: 1.8 sec, so the execution run time is about two seconds for all the model variations. We can infer that the models are equal as to the run-time.

4.4   Time resolution

The choice of time resolution is important as it decides to which extent reality can be modelled. Whereas batteries can, and often are modelled with a very high time resolution, this is normally not the case from an energy market perspective, where time resolution often follows the resolution of the price signals which incentivizes the use of flexibility.

In energy market modelling, a one-hour time resolution is normally chosen, and is sufficient for a high precision optimized decision. The lower the time resolution is, the less physics can be taken into account, as fluctuations in real life surroundings could potentially violate constraints on a short time basis, which are not violated when resolution is lower. This also means that the longer the duration is, the more decisions and responsibilities have to be handled by the local system. On the contrary, the higher the time resolution, the more data must be handled. This kind of data can be new and different forecasts/predictions like a weather update, the connection of new EVs, local decisions made due to fluctuations or unforeseen events etc.

In general, the time resolution should be equal to the factor that requires the highest resolution, which in a battery optimization case is not achievable. For example, an objective function maximizing the profit (savings) of a prosumer, will need to take load, PV production and price into account when deciding how to operate a battery, EV battery or other flexibility services. Although the price is updated on an hourly basis, the PV and load can change in a matter of seconds. With a high time resolution, fast changes in the system like an unexpected connection of an EV can be integrated quickly, whereas a low time resolution the EV will not be taken into account before a new time period starts.

The length of the time step has direct consequences on the model operation. The longer the time step, the more drastic the changes from one time step to another. Figure 30 shows the differences in SOE development when using 15-min (left panel) and one-hour (right panel) time step in otherwise identical models using the same input data. Figure illustrates that charging–discharging phenomena are the same qualitatively but the shorter time step makes all the changes more gradual, or the longer time step makes the SOE development more angular.
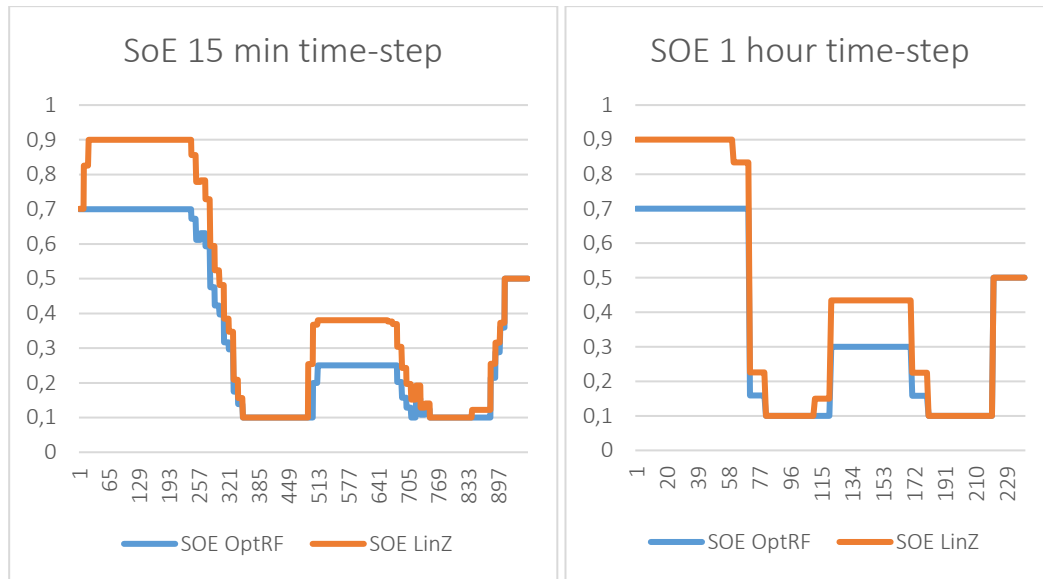
Figure 30. The impact of the length of the time-step on battery use. Left panel: 15-min time step. Right panel: one-hour time step.

4.5 Optimal operation regime

The optimal operation regime in terms of lifetime and performance can be defined based on the degradation stress factors, performance, and performance constraints. Based on the results from Sections 2.1, 2.3, 2.5, 3.4, 4.2, and 4.3, the following suggestions are made:

1. The operating temperature should stay within 15–30°C.

2. The E-rate should be fairly low (but not too low), preferably within E/5–E/2.

3. The SOE should be kept within 10–70% for most of the time.

4. The typical cycle depth should be fairly low, preferably less than 30%.

In case the proposed modelling method regarding the cost of degradation presented in Section 4.3 is implemented in the flexibility management operation algorithm, the item #4 is addressed automatically. However, the items #1–3 are not directly included in the cost of degradation nor any of the power constraints using the default parameters presented in Section 4.6.

4.6 Parameter extraction

Parameter extraction is based on the technical specifications, data sheets, cost information, and typical performance and degradation behaviour of the cell chemistry.

4.6.1 Energy capacity

Nominal installed energy capacity expressed in kWh specified in the data sheet of the ESS and defined on the ES-side shall be used.

4.6.2 Discharging power capacity

The nominal continuous discharging power of the ESS defined on the AC-side and expressed in kW shall be used.

In case the system does not have a common specification, the maximum charge and discharge power need to be defined. For the PCS, the maximum AC power is specified in the data sheet. For the battery, the battery-limited AC-power can be approximated as follows:

$$P_{\text{b,ac}}^{\text{dch}} = \eta_{\text{inv}}^{\text{dch}} P_{\text{b,dc}}^{\text{dch}} \tag{49}$$

where the $P_{\text{b,dc}}^{\text{dch}}$ is the maximum discharge power at a selected voltage. Conservative ratings are obtained if the low cut-off voltage, i.e., the minimum voltage, is used for both discharging and charging. With this selection, the specified AC power can always be provided regardless of the SOE and SOH.

$$P_{\text{b,ac}}^{\text{dch}} = \eta_{\text{inv}}^{\text{dch}} U_{\text{cut-off}}^{\text{dch}} I_{\text{n}}^{\text{dch}} \tag{50}$$

The minimum value shall be selected:

$$P^{\text{dch}} = \min\left\{ P_{\text{b,ac}}^{\text{dch}}, P_{\text{inv}} \right\} \tag{51}$$

4.6.3 Charging power capacity

The nominal continuous charging power of the ESS defined on the AC-side and expressed in kW shall be used.

In case the system does not have a common specification, the maximum charging power needs to be defined. The procedure is similar to the one presented in the previous Section for discharging power capacity. The equations for charging corresponding to Equations (49)–(51) are as follows:

$$P_{\text{b,ac}}^{\text{ch}} = \frac{P_{\text{b,dc}}^{\text{ch}}}{\eta_{\text{inv}}^{\text{ch}}} \tag{52}$$

$$P_{\text{b,ac}}^{\text{ch}} = \frac{U_{\text{cut-off}}^{\text{dch}} I_{\text{n}}^{\text{ch}}}{\eta_{\text{inv}}^{\text{ch}}} \tag{53}$$

$$P^{\text{ch}} = \min\left\{P_{\text{b,ac}}^{\text{ch}}, P_{\text{inv}}\right\} \tag{54}$$

4.6.4 Charging and discharging efficiencies

Total charging efficiency and discharging efficiency of the ESS include both the ES and the PCS. The specification provides typically only the optimal roundtrip energy efficiency, which is obtained at a low E-rate (typically in the range of E/5–E/2). Therefore, the anticipated average efficiency is calculated by using the estimated efficiency of the battery based on the methods presented in Section 2.1.2 and the efficiency chart of the inverter. If the inverter efficiency chart is not provided by the storage system supplier, the generic efficiency chart shown in Figure 13 may be used. The maximum value of the inverter efficiency curve can be adjusted to match the specified value by scaling the curve.

4.6.5 Cycle lifetime

A cycle life vs ∆DOD chart shall be requested from the storage supplier and implemented as a look-up table or as a mathematical function. If it is not provided, a generic chart shown in Figure 10 and presented in Equation (8) shall be used.

4.6.6 Replacement battery cost

A replacement battery cost expressed in k€ shall be used. The cost should include installation and all related costs, and it can be extracted from the offer. Anticipated cost decline may be applied. Estimates for the cost decline were given in Section 3.5.

4.6.7 Minimum SOE

A minimum SOE expressed in percentage shall be defined. It can be selected arbitrarily. Default value is 5%.

4.6.8 Maximum SOE

A minimum SOE expressed in percentage shall be defined. It can be selected arbitrarily. Default value is 95%.

4.6.9   End of constant-power region for charging

The end of constant-power region for charging expressed in percentage SOE shall be defined. It depends on the E-rate, and hence, it is convenient to define it for a specified E-rate and then to extrapolate it to comply with the rated charging power. Default value is 85% specified at a rate of 1E.

4.6.10 End of constant-power region for discharging

The end of constant-power region for charging expressed in percentage SOE shall be defined. It depends on the E-rate, and hence, it is convenient to define it for a specified E-rate and then to extrapolate it to comply with the rated discharging power. Default value is 10% specified at a rate of 1E.

4.6.11 Minimum power

Minimum power expressed in % of rated power.

References

[1] S. Ø. Ottesen, P. Olivella-Rosell, P. Lloret, A. Hentunen, P. Crespo del Granado, S. Bjarghov, V. Lakshmanan, J. Aghaei, M. Korpås and H. Farahmand, "Simplified Battery operation and control algorithm," Deliverable D5.3, EU-INVADE, 2017.

[2] M. Korpås, H. Farahmand and P. Crespo del Granado, "Methods for assessing the value of flexibility in distribution grids," Deliverable D5.2, EU-INVADE, 2017.

[3] A. Hentunen, V. Erkkilä and S. Jenu, "Storage system dimensioning and design tool," Deliverable D6.1, EU-INVADE, 2017.

[4] P. Lloret, P. Olivella, G. T. Berger, J. Timbergen and P. Rademakers, "Overall INVADE architecture," Deliverable D4.1, EU-INVADE, 2017.

[5] P. Lloret and P. Olivella, "INVADE architecture of pilots," Deliverable D4.2, EU-INVADE, 2017.

[6] C. Cordobés, "Pilot specifications," Deliverable D10.1, EU-INVADE, 2017.

[7] S. Jenu, A. Hentunen, S. Tuurala and A. Manninen, "Simplified state of health diagnostics tool, D6.3 EU-INVADE," 2018.

[8] D. Linden, Linden's Handbook of Batteries, 4th ed., T. B. Reddy, Ed., McGraw-Hill, 2011.

[9] A. Eddahech, O. Briat and J.-M. Vinassa, "Performance comparison of four lithium-ion battery technologies under calendar aging," *Energy,* vol. 84, pp. 542-550, 2015.

[10] J. T. Warner, The Handbook of Lithium-Ion Battery Pack Design, Elsevier, 2015.

[11] Puget Sound Energy, "2015 Integrated Resource Plan - Appendix L," 2015.

[12] D.-I. Stroe, M. Swierczynski, A.-I. Stan, R. Teodorescu and S. J. Andreasen, "Accelerated Lifetime Testing Methodology for Lifetime Estimation of Lithium-Ion

Batteries Used in Augmented Wind Power Plants," *IEEE Transactions on Industry Applications,* vol. 50, no. 6, pp. 4006-4017, 2014.

[13] P. T. Moseley and J. Garche, Eds., Electrochemical Energy Storage for Renewable Sources and Grid Balancing, Elsevier, 2014.

[14] T. Waldmann, G. Bisle, B.-I. Hogg, S. Stumpp, M. A. Danzer, M. Kasper, P. Axmann and M. Wohlfart-Mehrens, "Influence of Cell Design on Temperatures and Temperature Gradients in Lithium-Ion Cells: An In Operando Study," *Journal of The Electrochemical Society,* vol. 162, no. 6, pp. A921-A927, 2015.

[15] W. Waag, S. Käbitz and D. U. Sauer, "Experimental investigation of the lithium-ion battery impedance characteristic at various conditions and aging states and its influence on the application," *Applied Energy,* vol. 102, pp. 885-897, 2013.

[16] J. F. Peters, M. Baumann, B. Zimmermann, J. Braun and M. Weil, "The environmental impact of Li-ion batteries and the role of key parameters - A review," *Renewable and Sustainable Energy Reviews,* vol. 67, pp. 491-506, 2017.

[17] A. Barré, B. Deguilhem, S. Grolleau, M. Gérard, F. Suard and D. Riu, "A review on lithium-ion battery ageing mechanisms and estimations for automotive applications," *Journal of Power Sources,* vol. 241, pp. 680-689, 2013.

[18] C. Birkl, M. Roberts, E. McTurk and P. Bruce, "Degradation diagnostics for lithium ion cells," *Journal of Power Sources,* vol. 341, pp. 373-386, 2017.

[19] M. Jäger, A. Awarke, J. Bockstette and J. Ogrzewalla, "Thermal Management for Lithium-Ion-Batteries: Trade-off Between Driving Range, Lifetime and Performance," in *21st Aachen Colloquium Automobile and Engine Technology*, Aachen, 2012.

[20] V. Ruiz, A. Kriston, A. Pfang and L. Brett, "Deliverable #2: Overview of standardised battery ageing methods and summary of battery degradation processes," European Commission, Joint Research Centre (JRC), Directorate for Energy, Transport and Climate, 2016.

[21] N. Omar, M. Monem, Y. Firouz, J. Saminen, J. Smekens, O. Hegazy, H. Gaulons, G. Mulder, P. Van den Bossche, T. Coosemans and J. Van Mierlo, "Lithium iron

phosphate based battery – Assessment of the aging parameters and development of cycle life model," *Applied Energy,* vol. 113, pp. 1575-1585, 2014.

[22] M. Ecker, N. Nieto, S. Käbitz, J. Schmalstieg, H. Blanke, A. Warnecke and D. Sauer, "Calendar and cycle life study of Li(NiMnCo)O2-based 18650 lithium-ion batteries," *Journal of Power Sources,* vol. 248, pp. 839-851, 2014.

[23] S. Käbitz, J. Gerschler, M. Ecker, Y. Yurdagel, B. Emmermacher, D. André, T. Mitsch and D. Sauer, "Cycle and calendar life study of a graphite|LiNi1/3Mn1/3Co1/3O2 Li-ion high energy system. Part A: Full cell characterization," *Journal of Power Sources,* vol. 239, pp. 572-583, 2013.

[24] J. Wang, J. Purewal, P. Liu, J. Hicks-Garner, S. Soukazian, E. Sherman, A. Sorenson, L. Vu, H. Tataria and M. Verbrugge, "Degradation of lithium ion batteries employing graphite negatives and nickel cobalt manganese oxide + spinel manganese oxide positives: Part 1, aging mechanisms and life estimation," *Journal of Power Sources,* vol. 269, pp. 937-948, 2014.

[25] S. Saxena, C. Hendricks and M. Pecht, "Cycle life testing and modeling of graphite/LiCoO2 cells under different state of charge ranges," *Journal of Power Sources,* vol. 237, pp. 394-400, 2016.

[26] E. Sarasketa-Zabala, I. Gandiaga, E. Martinez-Laserna, L. Rodriguez-Martinez and I. Villareal, "Cycle ageing analysis of a LiFePO4/graphite cell with dynamic model validations: Towards realistic lifetime predictions," *Journal of Power Sources,* vol. 275, pp. 573-587, 2015.

[27] Saft, "Li-ion battery life - Technical sheet," May 2014. [Online]. Available: https://www.saftbatteries.com. [Accessed 13 February 2018].

[28] Y. Wang, Z. Zhou, A. Botterud, K. Zhang and Q. Ding, "Stochastic coordinated operation of wind and battery energy storage system considering battery degradation," *Journal of Modern Power Systems and Clean Energy,* vol. 4, no. 4, pp. 581-592, 2016.

[29] J. Peters, M. Baumann, B. Zimmermann, J. Braun and M. Weil, "The environmental impact of Li-Ion batteries and the role of key parameters - A review," *Renewable and Sustainable Energy Reviews,* vol. 67, pp. 491-506, 2017.

[30] S. Saxena, C. Le, J. Macdonald and Moura, S., "Quantifying EV battery end-of-life through analysis of travel needs with vehicle powertrain models," *Journal of Power Sources,* vol. 282, pp. 265-276, 2015.

[31] M. O. Ramoni and H. Zhang, "End-of-life (EOL) issues and options for electric vehicle batteries," *Clean Technologies and Environmental Policy,* vol. 15, no. 6, pp. 881-891, 2013.

[32] United States Advanced Battery Consortium (USABC), *Electric vehicle battery test procedures manual, revision 2,* 1996.

[33] *Secondary lithium-ion cells for the propulsion of electric road vehicles - Part 1: Performance testing,* IEC 62660-1, 2010.

[34] *Secondary cells and batteries containing alkaline or other non-acid electrolytes – Secondary lithium cells and batteries for use in industrial applications,* IEC 62620, 2014.

[35] *Secondary cells and batteries containing alkaline or other non-acid electrolytes – Secondary lithium cells and batteries for portable applications,* IEC 61960, 2011.

[36] T. Waldmann, J. B. Quinn, K. Richter, M. Kasper, A. Tost, A. Klein and M. Wohlfahrt-Mehrens, "Electrochemical, Post-Mortem, and ARC Analysis of Li-Ion Cell Safety in Second-Life Applications," *Journal of The Electrochemical Society,* vol. 164, no. 13, pp. A3154-A3162, 2017.

[37] L. Canals Casals, B. Amante Garcia, F. Aguesse and A. Iturrondobeitia, "Second life of electric vehicle batteries: relation between materials degradation and environmental impact," *International Journal of Life Cycle Assessment,* vol. 22, pp. 82-93, 2017.

[38] IRENA, "Battery Storage for Renewables: Market Status and Technology Outlook," 2015.

[39] TESVOLT, "TS HV data sheet," [Online]. Available: http://www.tesvolt.com/templates/tesvolt/files/pdf/E.DB.TSHV.ENG-A.20.pdf. [Accessed 21 February 2018].

[40] BYD, "B-Box Pro data sheet," [Online]. Available: http://www.byd.com/energy/download/low-voltage/B-Box Low Voltage Specification.pdf. [Accessed 21 February 2018].

[41] M. Schimpe, M. Naumann, N. Truong, H. C. Hesse, S. Santhanagopalan, A. Saxon and A. Jossen, "Energy efficiency evaluation of a stationary lithium-ion battery container storage system via electro-thermal modeling and detailed component analysis," *Applied Energy,* vol. 210, pp. 211-229, 2018.

[42] SMA Solar Technology AG, *Technical Information - Efficiency and Derating: SUNNY BOY / SUNNY BOY STORAGE / SUNNY TRIPOWER / SUNNY MINI CENTRAL v4.3.*

[43] M. Steen, N. Lebedeva, F. Di Persio and L. Boon-Brett, "EU Competitiveness in Advanced Batteries for E-Mobility and Stationary Storage Applications – Opportunities and Action," EUR 28837 EN, Publications Office of the European Union, Luxembourg, 2017.

[44] B. Nykvist and M. Nilsson, "Rapidly falling costs of battery packs for electric vehicles," *Nature Climate Change,* vol. 5, pp. 329-332, 2015.

[45] Deutsche Bank Markets Research, "EV battery makers," 2016.

[46] A. Hentunen, Electrical and thermal characterization of large lithium-ion batteries for non-road mobile machinery applications, D.Sc. (Tech.) dissertation, Aalto University, 2016.

[47] B. Xu, J. Zhao, T. Zheng, E. Litvinov and D. S. Kirschen, "Factoring the Cycle Aging Cost of Batteries Participating in Electricity Markets," *IEEE Transactions on Power Systems,* 2017.

[48] M. A. Ortega-Vazquez, "Optimal scheduling of electric vehicle charging and vehicle-to-grid services at household level including battery degradation and price

uncertainty," *IET Generation, Transmission & Distribution,* vol. 8, no. 6, pp. 1007-1016, 2014.